

Thermal-Drift Sampling: Generating Thermal Ensembles for Learning Many-Body Systems

Jiyu Jiang,¹ Mingrui Jing,¹ Jizhe Lai,¹ Xin Wang,^{1,*} and Lei Zhang¹

¹*Thrust of Artificial Intelligence, Information Hub,*

The Hong Kong University of Science and Technology (Guangzhou), Guangzhou 511453, China

(Dated: March 20, 2026)

Thermal equilibrium states of many-body Hamiltonians are essential for probing quantum chaos, finite-temperature phases of matter, and training quantum machine learning models, yet generating large collections of such states across different Hamiltonians remains costly with existing methods. We introduce a powerful operation, the quantum thermal-drift channel, to construct a measurement-controlled sampling algorithm that autonomously generates thermal states together with their system Hamiltonians as labels for general physical models. We prove that our algorithm is efficient: the total gate count scales polynomially with system size and quadratically with inverse temperature, providing the first polynomial resource bound for random thermal state generation. We characterize the distribution of sampled Hamiltonians as a normal distribution reweighted by partition functions, which quantifies a trade-off between sampling accuracy and effective label range. Level-spacing statistics computed from sampled thermal states of a 2D transverse-field Ising model show a crossover to Wigner–Dyson universality, confirming that the sampler captures nontrivial chaotic correlations. Finally, a variational quantum classifier trained on the generated dataset achieves near-optimal accuracy in predicting Hamiltonian properties of unseen states. These results establish a scalable, quantum-native route for thermodynamic simulation and labeled quantum data generation in many-body systems.

Introduction.— Random quantum states are a fundamental resource in quantum information science [1] which exhibit universal entanglement and spectral properties predicted by random matrix theory, making them indispensable for benchmarking quantum devices [2, 3] and probing the limits of classical simulability [4, 5]. They are essential for understanding quantum chaos [6] and black-hole physics [7], and serve as testbeds for quantum supremacy [8, 9] and device characterization [10]. Recently, the rise of quantum machine learning has created a new demand for these states [11]. Large collections of quantum states are treated as “quantum data” to learn the underlying patterns of many-body systems [12, 13].

The random-state families studied so far, such as Haar-random states [14], unitary t -designs [15], and random stabilizer states [16], consist of pure states whose statistical properties are determined by the geometry of Hilbert space alone, without reference to a specific physical Hamiltonian. Thermal states describe realistic many-body systems at finite temperature, exhibiting highly nontrivial correlations and often volume-law entanglement, making them representative of the “typical” mixed states encountered in quantum chaos and finite-temperature phases [10]. They allow us to probe the eigenstate thermalization hypothesis [17] and spectral statistics governed by random matrix theory [1]. Random thermal states therefore constitute a physically grounded family for probing universal many-body phenomena, motivating the development of efficient generation methods that do not rely on detailed spectral knowledge nor classical simulation. Beyond preparing a single thermal state, data-driven applications such as Hamiltonian learning and quantum device benchmarking demand a large, labeled collection: many thermal states, each paired with the Hamiltonian from which it was generated. Producing such paired data $(G_{\beta,H}, H)$ at scale is a important challenge for supervised learning with quantum data.

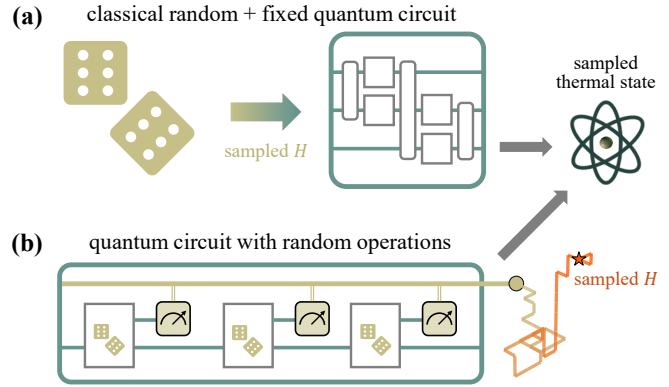


Fig 1. Difference between classical sampling and measurement-controlled sampling. The task is to sample a thermal state together with its Hamiltonian label. (a) Sampling the label via classical computers. The thermal state is prepared using existing thermal-state preparation circuits. (b) Sampling the thermal state and label via one structured random circuit. The label is generated by a lattice walk based on outcomes of mid-circuit measurements.

With quantum processors advancing toward the early fault-tolerant regime, efficient algorithms for thermal state preparation on quantum hardware are increasingly sought after. Practical generation of random thermal states, however, remains costly with existing both classical and quantum algorithms. Classical methods either suffer from the sign problem [18] or exhibit volume-law entanglement that makes classical contraction costs grow exponentially with system size [19]. Current quantum methods rely on quantum phase estimation combined with imaginary-time evolution [20–24], fluctuation theorems [25], or quantum Metropolis and Lindbladian thermalization algorithms [26–37] that couple the system to an effective bath. These instance-oriented methods can be effective for preparing one thermal state, but do not directly address the task of sampling thermal states from a family of Hamiltonians.

* felixxinwang@hkust-gz.edu.cn

TABLE I. Resource complexity for generating a thermal state together with its Hamiltonian label H . Here n , β , λ , ϵ , and δ denote the number of qubits, inverse temperature, sum of coefficient bounds, target precision, and failure probability. t_{mix} denotes the mixing time of a β -dependent Markov chain determined by the sampled H . Note that the prior methods were designed for preparing the thermal state of a single given Hamiltonian; the listed complexities reflect the cost of combining them with a classical label-sampling step, rather than producing $(G_{\beta,H}, H)$ as an ensemble-level generation algorithm.

Workflow	Query model	Complexity
Sample label + prepare state	Block encoding of normalized H [22]	$\mathcal{O}(2^{n/2}\lambda\beta/\text{Tr}[e^{-\beta H}])$
	Block encodings of jump operators [33]	$\mathcal{O}(\beta t_{\text{mix}})$
Sample state with label	Elementary gates (this work)	$\mathcal{O}(n^2\lambda^2\beta^2\epsilon^{-2/3}\log(1/\delta))$

Extending them to random thermal ensembles requires reconfiguring the circuit for each Hamiltonian instance, incurring substantial classical overhead that limits scalability.

In this Letter, we solve this critical problem by introducing a quantum algorithm for the scalable generation of random thermal states with provable polynomial efficiency, as illustrated in Figure 1. The device is programmed solely with a target set of L Pauli operators $\Sigma = \{\sigma_1, \dots, \sigma_L\}$ representing the interaction topology. Our algorithm autonomously generates the thermal state $G_{\beta,H} = e^{-\beta H}/\text{Tr}[e^{-\beta H}]$ together with its label $H = \sum c_j \sigma_j$, with coefficients c_j drawn from a thermal-weighted normal distribution, effectively functioning as a stochastic subroutine. Conceptually, the circuit performs a measurement-driven random walk in Hamiltonian space while approximately thermalizing the system state; the same measurement record that steers the evolution also specifies the Hamiltonian label.

Our algorithm operates as a measurement-controlled sampling protocol that applies a sequence of thermal-drift channels to generate the target thermal state. Unlike previous instance-oriented approaches [22, 33], it provides the first explicit polynomial scaling of resource complexity with respect to all problem parameters in an elementary-gate model, as summarized in Table I. The thermal-drift channel introduced here converts mid-circuit measurement randomness directly into physically meaningful Hamiltonian parameters, unifying state preparation and Hamiltonian sampling in a single quantum protocol. Systematic benchmarking validates the predicted β -dependence and sampling efficiency. We further present two complementary applications of the sampler. First, level-statistics analysis confirms that the sampled states capture the spectral correlations characteristic of a chaotic regime. Second, as a proof of concept for quantum data generation, a variational quantum classifier trained on the sampled thermal states, illustrating that the sampler can directly provide labeled quantum datasets for learning tasks.

Generation of random thermal states.— The task is to sample a thermal ensemble which is composed of a thermal state $G_{\beta,H}$ as “data” together with its Hamiltonian H as “la-

bel”, and H is from a structured family of Pauli Hamiltonians. Given a set of L distinct n -qubit Pauli operators Σ and the inverse temperature $\beta > 0$, such family is described by a set of all linear combinations of operators in Σ with bounded coefficients as

$$\mathfrak{H} = \left\{ \sum_j c_j \sigma_j : |c_j| \leq h_j, c_j \in \mathbb{R}, \sigma_j \in \Sigma \right\}. \quad (1)$$

where h_j ’s are the boundary values of the coefficients. Unlike the pure-state families discussed in the introduction, our setting asks for generating a structured thermal state that is linked to an explicit physical Hamiltonian. This provides a controllable generating set essential for physical benchmarking and Hamiltonian learning.

This setting imposes no restrictions on the locality or commutativity of the interactions. Our verification experiments consider two physical models on a 3×3 two-dimensional grid, where two-local Pauli operators act on nearest-neighbor pairs. The first is a Heisenberg model with Σ containing operators of the form XX , YY , and ZZ ; the second is a transverse-field Ising model with Σ containing operators of the form ZZ and X (or XX and Z). For both models, the coefficient bounds h_j are uniform, and we denote $\lambda = \sum_j h_j$, which upper bounds the largest eigenvalue of any $H \in \mathfrak{H}$.

Quantum thermal-drift channel.— Ground state preparation is known to be QMA-hard in the worst case [38, 39], and low-temperature thermal state preparation faces comparable complexity barriers [40]. A standard ‘sample-then-prepare’ pipeline, which first selects a Hamiltonian H and subsequently attempts to prepare its thermal state, is therefore often prohibitively costly. To circumvent this, we implement quantum operations involving randomness directly on the quantum hardware.

We define the thermal-drift channel \mathcal{N}_σ for any Pauli operator σ , which is the core component of our algorithm. For any input state ρ , the channel is defined as

$$\mathcal{N}_\sigma(\rho) = \frac{\mu}{2} (|\uparrow\rangle\langle\uparrow| \otimes \mathcal{E}_\sigma^\uparrow(\rho) + |\downarrow\rangle\langle\downarrow| \otimes \mathcal{E}_\sigma^\downarrow(\rho)), \quad (2)$$

where $\mu < 1$ is a scaling factor. Here, for any state ρ , the maps $\mathcal{E}_\sigma^\uparrow$ and $\mathcal{E}_\sigma^\downarrow$ are two completely positive operations defined as $e^{+\tau\sigma/2}\rho e^{+\tau\sigma/2}$ and $e^{-\tau\sigma/2}\rho e^{-\tau\sigma/2}$, respectively, with a thermal strength $\tau > 0$. The first register of $\mathcal{N}_\sigma(\rho)$ induces a random branch. Measuring this flag register indicates which direction the state is thermalized toward, with probabilities proportional to the corresponding unnormalized traces.

The thermal-drift channel can be implemented using system-ancilla coupling in a dilated Hilbert space, followed by measuring and tracing out the flag register, such that the whole channel can be implemented within $\mathcal{O}(n)$ quantum elementary gates and $2n$ ancilla qubits. We refer to the Supplemental Material for a detailed implementation.

Thermal state generation algorithm.— Our algorithm is implemented as a circuit of N blocks applied to an initial state ρ_0 . In block k , a thermal-drift channel $\mathcal{N}_{\sigma_{jk}}$ is applied, where σ_{jk} is selected independently from the set Σ . The probability of choosing \mathcal{N}_{σ_j} is weighted by the bound h_j , so that the distribution is h_j/λ . The thermal strength is fixed across

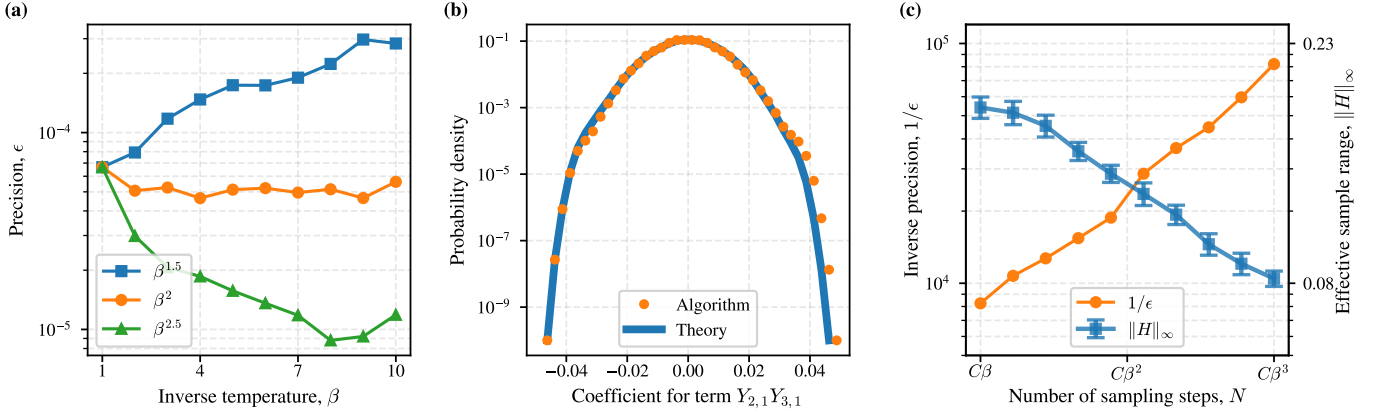


Fig. 2. Numerical verification of the theoretical predictions for the thermal-drift sampling algorithm applied to a 3×3 two-dimensional Heisenberg model. See the Supplemental Material for additional experimental details. (a) Precision ϵ between the output state and the ideal thermal state as a function of the inverse temperature β , for different step scalings. (b) Empirical marginal distribution of a nearest-neighbor YY interaction coefficient, compared with the theoretical prediction from Theorem 2. Here $Y_{i,j}$ denotes the Pauli- Y on the site at row i and column j . (c) Trade-off between inverse precision and effective sample range at fixed β , as the number of steps N increases from $C\beta$ to $C\beta^3$, where C is a fixed constant.

all blocks to $\tau = \beta\lambda/N$. After this thermal-drift channel, a measure-and-trace operation \mathcal{M}_{m_k} is applied to the flag register, generating a measurement outcome m_k . This outcome is recorded as $m_k \in \{+1, -1\}$ corresponding to \uparrow and \downarrow .

The full circuit implementation is labeled by an ordered list of values $\mathbf{j} = \{j_1, \dots, j_N\}$ and an ordered list of directions $\mathbf{m} = \{m_1, \dots, m_N\}$, that corresponds to a channel $\mathcal{E}_{\mathbf{j}, \mathbf{m}}$. In particular, one can collect the accumulated drift along each Pauli axis σ_j , which defines the overall Hamiltonian label

$$H_{\mathbf{j}, \mathbf{m}} = \frac{\lambda}{N} \sum_{j=1}^N \sum_{k: j_k=j} m_k \sigma_j. \quad (3)$$

When ρ_0 is the maximally mixed state, the output state $\mathcal{E}_{\mathbf{j}, \mathbf{m}}(\rho_0)$ is an approximate copy of its thermal state $G_{\beta, H_{\mathbf{j}, \mathbf{m}}}$, thereby completing the task of random thermal state generation.

Theoretical guarantees of sampling process.— Unlike randomized algorithms such as QDRIFT [41], where the randomness is Markovian and can be analyzed directly in channel form, each measurement outcome in our algorithm depends on the evolving state, and hence the process is generally non-Markovian. We apply matrix-martingale concentration inequalities to bound the sampling error, and lattice random-walk theory to characterize the induced distribution over Hamiltonian labels.

We start with the sampling error ϵ , quantified by the trace distance between the sampled state and the ideal thermal state. Given the sampled outcomes \mathbf{j} and \mathbf{m} , we consider the effective Hamiltonian H_\approx such that $\mathcal{E}_{\mathbf{j}, \mathbf{m}}(\rho_0) = e^{-\beta H_\approx} / \text{Tr}[e^{-\beta H_\approx}]$. Then the sampling error is bounded by $\epsilon \leq \beta \|H_{\mathbf{j}, \mathbf{m}} - H_\approx\|_\infty$. When the number of steps N is not large enough, the sampling error behaves like the discretization error of a second-order Trotter product formula [42], scaling as $\mathcal{O}(\beta^3)$. However, when N is sufficiently large so that Pauli operators are likely repetitive, we treat \mathbf{m} as random

variables conditional on a fixed \mathbf{j} . In this regime, the Freedman inequality for matrix martingales [43] implies an $\mathcal{O}(\beta^2)$ scaling almost surely. This is numerically verified in Figure 2(a). For increasing inverse temperature starting at $\beta = 1$, we test our algorithm with number of steps $N = \mathcal{O}(\beta^k)$ for $k = 1.5, 2$ and 2.5 , and observe that the average sampling error scales as $\mathcal{O}(\beta^{2-k})$, which is consistent with the following result. Here $\tilde{\mathcal{O}}(\cdot)$ omits the logarithm terms.

Theorem 1 (Sampling precision) *For any system size n , inverse temperature β , and sufficiently large N , our algorithm uses $\mathcal{O}(nN \log(1/\delta))$ gates to sample a thermal state and its label, with precision $\tilde{\mathcal{O}}(n^{3/2} \lambda^3 \beta^3 N^{-3/2})$ and failure probability at most δ .*

This result guarantees that the gate resources required by the sampler scale polynomially in all problem parameters. The cubic dependence on β reflects the accumulation of discretization error in the second-order Trotter product formula. Then as the number of thermal-drift steps N increases, the trace-distance error between the sampled state and the target thermal state decreases as $N^{-3/2}$, providing a route to higher-fidelity sampling.

To obtain a theoretical analysis of the sample distribution, we consider an asymptotic regime where the number of sampling steps N tends to infinity, so that every possible label $H \in \mathfrak{H}$ can be sampled. Then our algorithm can be modeled as a random walk $(\mathbf{x}^{(k)})_k$ on an L -dimensional integer lattice \mathbb{Z}^L , such that $\mathbf{x}^{(0)}$ and $\mathbf{x}^{(N)}$ correspond to the identity matrix and the sampled label H , respectively. Such a walk sequence satisfies for all $k \geq 1$,

$$\Pr(\mathbf{x}^{(k)} - \mathbf{x}^{(k-1)} = \pm e_j) = \Pr(m_k = \pm 1) \cdot h_j / \lambda, \quad (4)$$

where e_j denotes the j -th unit vector. Applying lattice-based random walk theory [44] yields a Gaussian approximation to

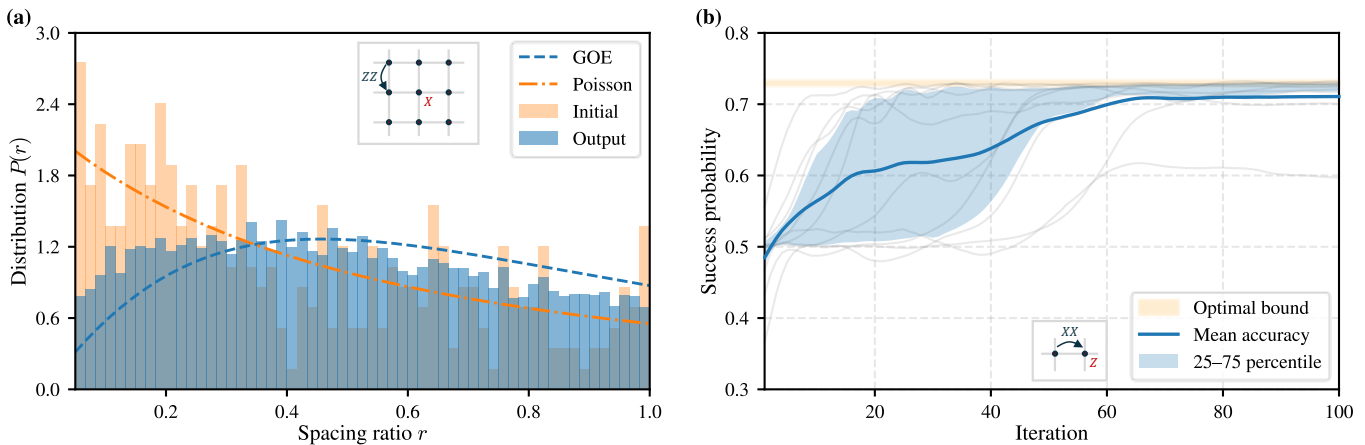


Fig 3. Applications of our thermal state sampler to level statistics and state classification. See the Supplemental Material for additional experimental details. **(a)** Level-spacing ratio statistics of the sampled thermal states for a 3×3 two-dimensional transverse-field Ising model. The orange histogram in the background corresponds to the initial state, while the blue histogram in the foreground corresponds to the output state generated by the sampling algorithm. The dashed curve indicates the GOE prediction, and the dash-dotted curve indicates the Poisson prediction. See the *Application to signatures of quantum chaos* section for task details. **(b)** Classification accuracy of a quantum classifier trained on sampled thermal states of a two-qubit Ising model. Gray traces show individual trial runs, the blue curve shows the mean success probability across independent test sets over 10 trials, the shaded region marks the 25–75 percentile band, and the orange band indicates the range of theoretical upper bound on success probability. See the *Application to state classification* section for task details.

the endpoint distribution under appropriate scaling. Combined with the thermal reweighting from $\Pr(m_k = \pm 1)$, the sampling rule takes a product form involving the partition function and a normal density.

Theorem 2 (Label distribution) *For any inverse temperature β , a label $H \in \mathcal{H}$ can be asymptotically sampled by our algorithm with probability proportional to $\text{Tr}[e^{-\beta H}] D(\mathbf{x})$, where D is an L -dimensional multivariate normal distribution and \mathbf{x} satisfies $\mathbf{x}_j = \text{Tr}[H\sigma_j]/\lambda \cdot N$.*

The sampling probability is governed by two factors. The partition-function weight $\text{Tr}[e^{-\beta H}]$ biases the sampler toward Hamiltonians with more thermally accessible states, i.e., those with lower free energy at the given temperature. The normal density $D(\mathbf{x})$ arises from the central-limit behavior of the underlying lattice random walk and concentrates the sampled coefficients near the origin. Together, they define a physically motivated measure over the Hamiltonian family.

We numerically show that a similar result holds in non-asymptotic cases. Taking $\beta = 2$, we sample from our algorithm and visualize one-dimensional slices of the marginal distribution of a chosen Pauli coefficient. As shown in Figure 2(b), the empirical distribution closely matches the ideal one. Note that the difference mainly occurs in both ends of the distribution, which will get smaller as the number of sampling step further increases.

We apply Theorems 1 and 2 to identify a trade-off between the sampling accuracy and the effective range of sampled Hamiltonians. Due to the nature of random walks, higher accuracy comes with a more concentrated label distribution, and vice versa. As shown in Figure 2(c), for $\beta = 2$, as the number of steps N increases from $\mathcal{O}(\beta)$ to $\mathcal{O}(\beta^3)$, the inverse precision $1/\epsilon$ increases while the effective sample range $\|H\|_\infty$

decreases at a similar rate. Therefore, despite the efficiency of a single execution, it is not recommended to use our algorithm for preparing thermal states of one fixed Hamiltonian. However, this characteristic makes our algorithm particularly well-suited for ensemble-level applications.

Application to signatures of quantum chaos.— Level statistics characterizes thermodynamic phases in quantum many-body systems [45] by probing spectral correlations of quantum states. Applying this analysis to thermal states across different Hamiltonians requires generating those states efficiently, a capability that our sampler can provide. Given any random density operator with an ordered many-body eigenvalue spectrum $\{\lambda_j\}_j$, one defines the adjacent logarithmic level spacings $\delta_j = \log(\lambda_j/\lambda_{j+1})$ and the dimensionless spacing (gap) ratio [46, 47],

$$r_j = \frac{\min\{\delta_j, \delta_{j+1}\}}{\max\{\delta_j, \delta_{j+1}\}} \in [0, 1], \quad (5)$$

whose distribution is insensitive to spectral unfolding and thus widely used in finite-size studies [5, 48, 49]. In ergodic systems satisfying the eigenstate thermalization hypothesis, strong level repulsion leads to Wigner–Dyson statistics [49, 50], whereas in the many-body localization phase, emergent local integrals of motion suppress correlations and produce Poisson level statistics [1, 51]. The Wigner–Dyson distribution describes the probability of the spacing ratio in the Gaussian orthogonal ensemble (GOE), serving as the universal signature of chaos for quantum systems that preserve time-reversal symmetry [48, 52].

To assess the chaotic nature of the generated states, we apply our algorithm to the level statistics of the sampled thermal state ensemble. An initial reference state whose spectrum exhibits near-Poisson statistics is compared with the output

states produced by the sampler. As shown in Figure 3(a), aggregating $\{r_j\}_j$ over samples yields a robust, unfolding-free diagnostic. The level statistics shift from a Poissonian distribution in the reference state to a Wigner–Dyson distribution in the output thermal ensemble, confirming that the sampler captures the spectral correlations of the ergodic regime. The thermal-drift mechanism thus drives the system into a substantially more chaotic sector of Hilbert space than the structured input, producing states whose spectral correlations are consistent with physical thermalization.

Application to state classification.— Our thermal state sampler provides a scalable data source for quantum supervised learning algorithms [53–55] that learn properties of quantum systems from their thermal states. Consider classifying a black-box quantum system with an unknown Hamiltonian $H \in \mathfrak{H}$ by a label function $f(H) \in \{0, 1\}$, given access to only a single copy of its thermal state. A natural approach is to deploy a variational quantum classifier [12, 13, 56] (VQC) on a large labeled dataset of thermal states. Theorem 1 implies that our sampler can generate such a dataset with cost polynomial in system size and inverse temperature, bypassing the need for individual state preparation. In the expectation-value-based formulation, training typically requires repeatedly measuring the same input state to estimate observables; here, we instead use single-shot measurements on freshly regenerated batches from the sampler, which is naturally compatible with a stochastic data source.

As a proof of concept, a VQC is trained to classify two-qubit Ising models described by $\Sigma = \{XX, ZI, IZ\}$ and $h = (1, 1, 1)$ according to the sign of the XX coefficient, where the optimal success probability is upper bounded by the Helstrom limit [57]. The classifier is optimized via a stochastic variant of the parameter-shift rule [58, 59]. In our implementation, each gradient evaluation uses single-shot measurements on a freshly regenerated batch of 10^3 approximate thermal states from our sampler. The classifier is evaluated, in each trial, on an independently generated test set of 3×10^3 exact thermal states. As shown in Figure 3(b), the prediction accuracy approaches the Helstrom limit in most trials, with noticeable trial-to-trial variability. In particular, the classifier trains on approximate states sampled from the thermal-weighted normal distribution (Theorem 2) yet generalizes to test states drawn from a uniform distribution. This distribution-shift robustness is enabled by the polynomial sampling cost (Theorem 1), which allows generating sufficiently large and diverse training sets without individual state preparation. Combined with the built-in Hamiltonian labeling, the sampler serves as an end-to-end data source for quantum supervised learning in this setting. See the Supplemental Material for training details.

Conclusion and outlook.— We have introduced the quantum thermal-drift channel and used it to develop a

measurement-controlled algorithm that generates random thermal states for Hamiltonians drawn from general Pauli models, with sampling cost polynomial in both the system size and the inverse temperature. This efficiency bypasses the high overhead of instance-oriented preparation methods and provides, to our knowledge, the first polynomial-cost quantum protocol for random thermal state generation. Two applications demonstrate the versatility of this approach: level-statistics analysis confirms that the sampled states exhibit Wigner–Dyson universality, a regime associated with strong level repulsion and quantum chaos; and a proof-of-concept classification experiment shows that the sampled dataset can serve as a data source for quantum learning tasks.

Several avenues for future research remain open. Our protocol relies on elementary gates and mid-circuit measurements, and can be viewed as a stochastic subroutine for generating labeled quantum data on early fault-tolerant devices. Improving the system-size scaling, potentially by exploiting structure in physically motivated Hamiltonian families, remains an important direction. We note that the polynomial efficiency achieved here contrasts with the known limitations of leading classical approaches for generic models: quantum Monte Carlo encounters the sign problem for frustrated systems [18], and tensor-network contractions incur costs that grow exponentially with the volume-law entanglement present in generic thermal states [19]. Formalizing this contrast into a rigorous quantum advantage proof remains an interesting open question. On the machine learning side, extending the classification framework to more complex Hamiltonians and scalable optimization strategies would further establish the practical utility of quantum-generated thermal state datasets.

Note added.— We recently became aware of related independent works [60, 61] that simulate thermal states by applying sequences of Pauli-based nonunitary updates starting from the maximally mixed state. These works focus on thermal state preparation for a given Hamiltonian via classical algorithms, whereas we focus on thermal state generation for random Hamiltonians via quantum circuits.

Acknowledgment.— The authors are listed in alphabetical order. This work was partially supported by the National Key R&D Program of China (Grant No. 2024YFB4504004), the National Natural Science Foundation of China (Grant No. 12447107, 92576114), the Guangdong Provincial Quantum Science Strategic Initiative (Grant No. GDZX2403008, GDZX2503001), the CCF-Tencent Rhino-Bird Open Research Fund, and the Guangdong Provincial Key Lab of Integrated Communication, Sensing and Computation for Ubiquitous Internet of Things (Grant No. 2023B1212010007).

Code availability.— Numerical experiments are based on an open-source Python research software for quantum computing [62]. Code and data used in the numerical experiments are available on <https://github.com/QuAIR/SamplingThermalState-Codes>.

[1] Vedika Khemani, S. P. Lim, D. N. Sheng, and David A. Huse. Critical properties of the many-body localization transition.

- [2] Christoph Dankert, Richard Cleve, Joseph Emerson, and Etera Livine. Exact and approximate unitary 2-designs and their application to fidelity estimation. *Phys. Rev. A*, 80:012304, 2009.
- [3] Easwar Magesan, J. M. Gambetta, and Joseph Emerson. Scalable and robust randomized benchmarking of quantum processes. *Phys. Rev. Lett.*, 106(18):180504, 2011.
- [4] Jonas Maziero. Random sampling of quantum states: A survey of methods. *Braz. J. Phys.*, 45(6):575–583, 2015.
- [5] J. Odavić, G. Torre, N. Mijić, D. Davidović, F. Franchini, and S. M. Giampaolo. Random unitaries, robustness, and complexity of entanglement. *Quantum*, 7:1115, 2023.
- [6] Joonhee Choi, Adam L. Shaw, Ivaylo S. Madjarov, Xin Xie, Ran Finkelstein, Jacob P. Covey, Jordan S. Cotler, Daniel K. Mark, Hsin-Yuan Huang, Anant Kale, Hannes Pichler, Fernando G. S. L. Brandão, Soonwon Choi, and Manuel Endres. Preparing random states and benchmarking with many-body quantum chaos. *Nature*, 613(7944):468–473, 2023.
- [7] Patrick Hayden and John Preskill. Black holes as mirrors: quantum information in random subsystems. *J. High Energy Phys.*, 2007(09):120, 2007.
- [8] Sergio Boixo, Sergei V. Isakov, Vadim N. Smelyanskiy, Ryan Babbush, Nan Ding, Zhang Jiang, Michael J. Bremner, John M. Martinis, and Hartmut Neven. Characterizing quantum supremacy in near-term devices. *Nat. Phys.*, 14(6):595–600, 2018.
- [9] Frank Arute, Kunal Arya, Ryan Babbush, and et. al. Quantum supremacy using a programmable superconducting processor. *Nature*, 574(7779):505–510, 2019.
- [10] Tong Liu, Shang Liu, Hekang Li, Hao Li, Kaixuan Huang, Zhongcheng Xiang, Xiaohui Song, Kai Xu, Dongning Zheng, and Heng Fan. Observation of entanglement transition of pseudo-random mixed states. *Nat. Commun.*, 14(1):1971, 2023.
- [11] Marco Cerezo, Guillaume Verdon, Hsin-Yuan Huang, Lukasz Cincio, and Patrick J. Coles. Challenges and opportunities in quantum machine learning. *Nat. Comput. Sci.*, 2(9):567–576, 2022.
- [12] Jonas Jäger and Roman V. Krems. Universal expressiveness of variational quantum classifiers and quantum kernels for support vector machines. *Nat. Commun.*, 14(1):576, 2023.
- [13] Daniel Flam-Shepherd, Tony C. Wu, Xuemei Gu, Alba Cervera-Lierta, Mario Krenn, and Alan Aspuru-Guzik. Learning interpretable representations of entanglement in quantum optics experiments using deep generative models. *Nat. Mach. Intell.*, 4(6):544–554, 2022.
- [14] Zhengfeng Ji, Yi-Kai Liu, and Fang Song. Pseudorandom quantum states. In *Annual International Cryptology Conference*, pages 126–152. Springer, 2018.
- [15] Joseph Emerson, Yaakov S Weinstein, Marcos Saraceno, Seth Lloyd, and David G Cory. Pseudo-random unitary operators for quantum information processing. *Science*, 302(5653):2098–2100, 2003.
- [16] Héctor J García, Igor L Markov, and Andrew W Cross. On the geometry of stabilizer states. *arXiv preprint arXiv:1711.07848*, 2017.
- [17] Luca D’Alessio, Yariv Kafri, Anatoli Polkovnikov, and Marcos Rigol. From quantum chaos and eigenstate thermalization to statistical mechanics and thermodynamics. *Adv. Phys.*, 65(3):239–362, 2016.
- [18] Matthias Troyer and Uwe-Jens Wiese. Computational complexity and fundamental limitations to Fermionic quantum Monte Carlo simulations. *Phys. Rev. Lett.*, 94(17):170201, 2005.
- [19] F. Verstraete, V. Murg, and J. I. Cirac. Matrix product states, projected entangled pair states, and variational renormalization group methods for quantum spin systems. *Adv. Phys.*, 57(2):143–224, 2008.
- [20] David Poulin and Pawel Wocjan. Sampling from the thermal quantum Gibbs state and evaluating partition functions with a quantum computer. *Phys. Rev. Lett.*, 103:220502, 2009.
- [21] Anirban Narayan Chowdhury and Rolando D. Somma. Quantum algorithms for Gibbs sampling and hitting-time estimation. *Quantum Inf. Comput.*, 17(1–2):41–64, 2017.
- [22] András Gilyén, Yuan Su, Guang Hao Low, and Nathan Wiebe. Quantum singular value transformation and beyond: Exponential improvements for quantum matrix arithmetics. In *Proceedings of the 51st Annual ACM SIGACT Symposium on Theory of Computing*, STOC 2019, page 193–204, New York, NY, USA, 2019. Association for Computing Machinery.
- [23] Mario Motta, Chong Sun, Adrian T. K. Tan, Matthew J. O’Rourke, Erika Ye, Austin J. Minnich, Fernando G. S. L. Brandão, and Garnet Kin-Lic Chan. Determining eigenstates and thermal states on a quantum computer using quantum imaginary time evolution. *Nat. Phys.*, 16(2):205–210, 2020.
- [24] Cambyse Rouzé, Daniel Stilck França, and Álvaro M. Alhambra. Optimal quantum algorithm for Gibbs state preparation, 2024.
- [25] Zoe Holmes, Gopikrishnan Muraleedharan, Rolando D. Somma, Yigit Subasi, and Burak Şahinoğlu. Quantum algorithms from fluctuation theorems: Thermal-state preparation. *Quantum*, 6:825, 2022.
- [26] Kristan Temme, Tobias J. Osborne, Karl G. Vollbrecht, David Poulin, and Frank Verstraete. Quantum Metropolis sampling. *Nature*, 471(7336):87–90, 2011.
- [27] Man-Hong Yung and Alán Aspuru-Guzik. A quantum-quantum Metropolis algorithm. *Proc. Natl. Acad. Sci. U.S.A.*, 109(3):754–759, 2012.
- [28] Jonathan E. Moussa. Low-depth quantum Metropolis algorithm, 2022.
- [29] Patrick Rall, Chunhao Wang, and Pawel Wocjan. Thermal state preparation via rounding promises. *Quantum*, 7:1132, 2023.
- [30] Oles Shtanko and Ramis Movassagh. Preparing thermal states on noiseless and noisy programmable quantum processors, 2023.
- [31] Pawel Wocjan and Kristan Temme. Szegedy walk unitaries for quantum maps. *Commun. Math. Phys.*, 402(3):3201–3231, 2023.
- [32] Chi-Fang Chen, Michael J. Kastoryano, Fernando G. S. L. Brandão, and András Gilyén. Quantum thermal state preparation, 2023.
- [33] Chi-Fang Chen, Michael J. Kastoryano, and András Gilyén. An efficient and exact noncommutative quantum Gibbs sampler, 2025.
- [34] Chi-Fang Chen, Michael Kastoryano, Fernando G. S. L. Brandão, and András Gilyén. Efficient quantum thermal simulation. *Nature*, 646(8085):561–566, 2025.
- [35] Zhiyan Ding, Bowen Li, and Lin Lin. Efficient quantum Gibbs samplers with Kubo–Martin–Schwinger detailed balance condition. *Commun. Math. Phys.*, 406(3):67, 2025.
- [36] Daniel Zhang, Jan Lukas Bosse, and Toby Cubitt. Dissipative quantum Gibbs sampling, 2023.
- [37] Fernando G. S. L. Brandão and Michael J. Kastoryano. Finite correlation length implies efficient preparation of quantum thermal states. *Commun. Math. Phys.*, 365(1):1–16, 2019.
- [38] John Watrous. *Quantum Computational Complexity*, pages 7174–7201. Springer New York, New York, NY, 2009.
- [39] Anirban N. Chowdhury, Guang Hao Low, and Nathan Wiebe. A variational quantum algorithm for preparing quantum Gibbs states, 2020.

- [40] Dorit Aharonov, Itai Arad, and Thomas Vidick. The quantum PCP conjecture, 2013.
- [41] Earl Campbell. Random compiler for fast Hamiltonian simulation. *Phys. Rev. Lett.*, 123(7):070503, 2019.
- [42] Andrew M. Childs, Dmitri Maslov, Yunseong Nam, Neil J. Ross, and Yuan Su. Toward the first quantum simulation with quantum speedup. *Proc. Natl. Acad. Sci. U.S.A.*, 115(38):9456–9461, 2018.
- [43] Joel A. Tropp. Freedman’s inequality for matrix martingales. *Electron. Commun. Probab.*, 16:262–270, 2011.
- [44] Frank Spitzer. *Principles of random walk*. Springer, New York, NY, 2001.
- [45] Andrew C. Potter, Romain Vasseur, and S. A. Parameswaran. Universal properties of many-body delocalization transitions. *Phys. Rev. X*, 5(3):031033, 2015.
- [46] Vadim Oganesyan and David A. Huse. Localization of interacting Fermions at high temperature. *Phys. Rev. B*, 75:155111, 2007.
- [47] Piotr Sierant and Jakub Zakrzewski. Model of level statistics for disordered interacting quantum many-body systems. *Phys. Rev. B*, 101(10):104201, 2020.
- [48] Maksym Serbyn and Joel E. Moore. Spectral statistics across the many-body localization transition. *Phys. Rev. B*, 93(4):041424, 2016.
- [49] Wouter Buijsman, Vadim Cheianov, and Vladimir Gritsev. Random matrix ensemble for the level statistics of many-body localization. *Phys. Rev. Lett.*, 122(18):180601, 2019.
- [50] Eugene P Wigner. Random matrices in physics. *SIAM review*, 9(1):1–23, 1967.
- [51] Arijet Pal and David A. Huse. Many-body localization phase transition. *Phys. Rev. B*, 82(17):174411, 2010.
- [52] D. A. Rabson, B. N. Narozhny, and A. J. Millis. Crossover from Poisson to Wigner–Dyson level statistics in spin chains with integrability breaking. *Phys. Rev. B*, 69(5):054403, 2004.
- [53] Adam Artymowicz. Efficient Hamiltonian learning from Gibbs states, 2024.
- [54] Chi-Fang Chen, Anurag Anshu, and Quynh T. Nguyen. Learning quantum Gibbs states locally and efficiently, 2025.
- [55] Andi Gu, Lukasz Cincio, and Patrick J. Coles. Practical Hamiltonian learning with unitary dynamics and Gibbs states. *Nat. Commun.*, 15(1):312, 2024.
- [56] Marcello Benedetti, Erika Lloyd, Stefan Sack, and Mattia Fiorentini. Parameterized quantum circuits as machine learning models. *Quantum Sci. Technol.*, 4(4):043001, 2019.
- [57] Carl W. Helstrom. Quantum detection and estimation theory. *J. Stat. Phys.*, 1(2):231–252, 1969.
- [58] Kosuke Mitarai, Makoto Negoro, Masahiro Kitagawa, and Keisuke Fujii. Quantum circuit learning. *Phys. Rev. A*, 98(3):032309, 2018.
- [59] Maria Schuld, Ville Bergholm, Christian Gogolin, Josh Izaac, and Nathan Killoran. Evaluating analytic gradients on quantum hardware. *Phys. Rev. A*, 99(3):032331, 2019.
- [60] Rafael Gómez-Lurbe and Armando Pérez. Pauli propagation for imaginary time evolution. *arXiv preprint arXiv:2601.14400*, 2026.
- [61] Manuel S. Rudolph, Armando Angrisani, Andrew Wright, Iwo Sanderski, Ricard Puig, and Zoë Holmes. Thermal state simulation with pauli and majorana propagation, February 2026.
- [62] QuAIR team. QuAIRKit. <https://github.com/QuAIR/QuAIRKit>, 2023.
- [63] Nicholas J. Higham. *Functions of Matrices*. Society for Industrial and Applied Mathematics, Philadelphia, PA, 2008.
- [64] Rajendra Bhatia and Hideki Kosaki. Mean matrices and infinite divisibility. *Linear Algebra Appl.*, 424(1):36–54, 2007. Special Issue in honor of Roger Horn.
- [65] Roger A. Horn and Charles R. Johnson. *Matrix analysis, 2nd Edition*. Cambridge University Press, Cambridge, United Kingdom, 2012.
- [66] Brian C. Hall. *Lie Groups, Lie Algebras, and Representations: An Elementary Introduction*. Springer, New York, US, 2015.
- [67] Y. Y. Atas, E. Bogomolny, O. Giraud, and G. Roux. Distribution of the ratio of consecutive level spacings in random matrix ensembles. *Physical Review Letters*, 110(8):084101, February 2013.

Supplemental Material for Thermal-Drift Sampling: Generating Thermal Ensembles for Learning Many-Body Systems

In this supplementary material, we offer detailed proofs of the theorems and propositions in the manuscript ‘Thermal-Drift Sampling: Generating Thermal Ensembles for Learning Many-Body Systems.’ In section A, we will introduce the notations and the basic lemmas that we used in the proofs and the analysis. We then, introduce the details of our thermal-drift channel in section B which serves as the core of our algorithm. After that, the fundamental setups of the random thermal state generation task and the algorithm statements are clarified in section C. We also provide performance and error analysis of our algorithm in the subsections of the same section. The applications towards the level statistics and the state classification are discussed in section D. The corresponding experimental details are provided in the followed section E for board interests.

Appendix A: Notations and Preliminaries

Asymptotic notations. Let $[N] = \{1, 2, \dots, N\}$ for any positive integer N . We use asymptotic notations to describe the scaling of complexity and error bounds. For two non-negative functions $f(x)$ and $g(x)$, we write $f(x) = \mathcal{O}(g(x))$ if there exist constants $C > 0$ and x_0 such that $f(x) \leq Cg(x)$ for all $x \geq x_0$. Conversely, $f(x) = \Omega(g(x))$ indicates that $f(x) \geq cg(x)$ for some constant $c > 0$ and sufficiently large x . The notation $f(x) = o(g(x))$ implies that $\lim_{x \rightarrow \infty} f(x)/g(x) = 0$. We also use the soft-O notation $\tilde{\mathcal{O}}(g(x))$ to suppress polylogarithmic factors, i.e., $\tilde{\mathcal{O}}(g(x)) \equiv \mathcal{O}(g(x) \text{ poly}(\log g(x)))$.

Operators. We denote the single-qubit Pauli operators by the set $\{I, X, Y, Z\}$, defined as $I = \begin{pmatrix} 1 & 0 \\ 0 & 1 \end{pmatrix}$, $X = \begin{pmatrix} 0 & 1 \\ 1 & 0 \end{pmatrix}$, $Y = \begin{pmatrix} 0 & -i \\ i & 0 \end{pmatrix}$ and $Z = \begin{pmatrix} 1 & 0 \\ 0 & -1 \end{pmatrix}$. The set of n -qubit Pauli operators is denoted as $\{I, X, Y, Z\}^{\otimes n}$. We denote the Hadamard gate and the single-qubit rotation around the y -axis by: $H = \frac{1}{\sqrt{2}} \begin{pmatrix} 1 & 1 \\ 1 & -1 \end{pmatrix}$ and $R_y(\theta) = e^{-i\theta Y/2} = \begin{pmatrix} \cos(\theta/2) & -\sin(\theta/2) \\ \sin(\theta/2) & \cos(\theta/2) \end{pmatrix}$. The commutator of operators A and B is $[A, B] = AB - BA$. The adjoint action (Lie bracket) is defined recursively as $\text{ad}_A(B) = [A, B]$ and $\text{ad}_A^k(B) = [A, \text{ad}_A^{k-1}(B)]$ for $k \geq 2$.

Quantum systems. Let \mathcal{H} denote a finite-dimensional complex Hilbert space. A density operator ρ is a linear operator acting on \mathcal{H} that is positive semi-definite matrix with unit trace, and we write $\mathcal{D}(\mathcal{H}_A)$ for the set of density operators on a system A with Hilbert space \mathcal{H}_A . For a composite system with Hilbert space $\mathcal{H}_{AB} = \mathcal{H}_A \otimes \mathcal{H}_B$, we write $X_A = X \otimes I_B$ to denote an operator X acting locally on subsystem A , where I_B is the identity on \mathcal{H}_B .

Norms. For a vector $\mathbf{x} = (x_1, \dots, x_L) \in \mathbb{C}^L$, we define the Euclidean norm as $\|\mathbf{x}\| = \sqrt{\sum_{i=1}^L |x_i|^2}$. For a matrix $A \in \mathbb{C}^{d \times d}$, we define the spectral norm $\|A\|_\infty$ as the largest singular value of A , and the trace norm $\|A\|_1$ as the sum of the singular values of A .

Parity functions. For $N \in \mathbb{N}$ and $\mathbf{x} = (x_1, \dots, x_L) \in \mathbb{Z}^L$, define the *reachability parity function* $a_N : \mathbb{Z}^L \rightarrow \{0, 2\}$ by

$$a_N(\mathbf{x}) = \begin{cases} 2, & \text{if } \sum_{j=1}^L |x_j| \leq N \text{ and } N - \sum_{j=1}^L |x_j| \text{ is even;} \\ 0, & \text{otherwise.} \end{cases} \quad (\text{A.1})$$

Thus $a_N(\mathbf{x}) = 0$ whenever \mathbf{x} is not reachable from the origin in N steps of the walk, and $a_N(\mathbf{x}) = 2$ otherwise. Define the *bitwise parity function* for $x \in \mathbb{N}$ as

$$p(x) = \begin{cases} 0, & \text{if } \sum_i x_i \text{ is even;} \\ 1, & \text{otherwise,} \end{cases} \quad (\text{A.2})$$

where $x_{N-1} \dots x_0$ is the binary representation of $x = \sum_i 2^i x_i$. Denote the first $l-1$ bits of x as $x_{1:l} := x_1 \dots x_{l-1}$.

Martingales. A *filtration* is a sequence of σ -algebras $\{\mathcal{F}_0, \mathcal{F}_1, \dots\}$ satisfying $\mathcal{F}_0 \subseteq \mathcal{F}_1 \subseteq \dots$. A sequence of random variables $\{X_k\}_{k \geq 0}$ is a *martingale* with respect to $\{\mathcal{F}_k\}$ if X_k is \mathcal{F}_k -measurable, $\mathbb{E}[|X_k|] < \infty$, and $\mathbb{E}[X_{k+1} | \mathcal{F}_k] = X_k$. A sequence $\{Y_k\}_{k \geq 1}$ is a *martingale difference sequence* (MDS) if it is adapted to the filtration and satisfies $\mathbb{E}[Y_{k+1} | \mathcal{F}_k] = 0$. An MDS is typically constructed from a martingale $\{X_k\}_k$ by setting $Y_k = X_k - X_{k-1}$.

1. Useful lemmas

This section collects auxiliary lemmas used in later proofs.

Lemma S1 (Fréchet derivative of matrix exponential, [63]) *Let A, E be two matrices. Then*

$$\frac{d}{dt} e^{A+tE} = \int_0^1 e^{s(A+tE)} E e^{(1-s)(A+tE)} ds. \quad (\text{A.3})$$

Lemma S2 *For any Hermitian matrix X and positive semidefinite matrix R ,*

$$\left\| \int_0^1 R^s X R^{1-s} ds \right\|_1 \leq \|X\|_\infty \|R\|_1 \quad (\text{A.4})$$

Proof Suppose R has the spectral decomposition $R = UDU^\dagger = \sum_j p_j |j\rangle\langle j|$ for some orthonormal basis $\{|j\rangle\}_j$. Denote $\mathcal{L}(X) = \int_0^1 D^s X D^{1-s} ds$. Consider the (i, j) th element of $\mathcal{L}(X)$:

$$\langle i | \mathcal{L}(X) | j \rangle = \langle i | \int_0^1 \sum_k p_k^s |k\rangle\langle k| X \sum_{k'} p_{k'}^{1-s} |k'\rangle\langle k'| ds | j \rangle \quad (\text{A.5})$$

$$= \langle i | X | j \rangle \int_0^1 p_i^s p_j^{1-s} ds \quad (\text{A.6})$$

$$= X_{i,j} L(p_i, p_j), \quad (\text{A.7})$$

where

$$L(a, b) = \begin{cases} a, & \text{if } a = b; \\ \frac{a-b}{\log a - \log b}, & \text{if } a \neq b. \end{cases} \quad (\text{A.8})$$

Denote the (i, j) th element of matrix \mathcal{L} as $L(p_i, p_j)$. The matrix \mathcal{L} is the Loewner matrix of the Schlicht function $\log z$ mapping the upper half-plane into itself [64], so \mathcal{L} is positive semidefinite (PSD). Since $\mathcal{L}(X) = X \odot \mathcal{L}$, where \odot is the Hadamard product, the Schur product theorem [65, Section 7.5] implies that $\mathcal{L}(X)$ is PSD whenever X is PSD. Therefore,

$$\mathcal{L}(\|X\|_\infty I) = \|X\|_\infty D \succeq \mathcal{L}(X) \succeq -\|X\|_\infty D = \mathcal{L}(-\|X\|_\infty I). \quad (\text{A.9})$$

Denote $\lambda_1(X), \lambda_2(X), \dots$ as the eigenvalues of X in ascending order. $\mathcal{L}(X) \succeq -\|X\|_\infty D$ means $-\lambda_j(\mathcal{L}(X)) \leq \|X\|_\infty \lambda_j(D)$ for all j satisfying $\lambda_j(\mathcal{L}(X)) < 0$, while $\|X\|_\infty D \succeq \mathcal{L}(X)$ means $\lambda_j(\mathcal{L}(X)) \leq \|X\|_\infty \lambda_j(D)$ for all j satisfying $\lambda_j(\mathcal{L}(X)) \geq 0$. Combining, we have

$$\|\mathcal{L}(X)\|_1 = \sum_j |\lambda_j(\mathcal{L}(X))| \leq \|X\|_\infty \sum_j \lambda_j(D) = \|X\|_\infty \|D\|_1 = \|X\|_\infty \|R\|_1. \quad (\text{A.10})$$

■

Lemma S3 (Baker–Campbell–Hausdorff formula for $e^X e^Y e^X$, [66]) *For matrices X and Y ,*

$$\log(e^X e^Y e^X) = 2X + Y - \frac{1}{6} [X + Y, [X, Y]] + \mathcal{O}(\|X\|_\infty + \|Y\|_\infty)^5). \quad (\text{A.11})$$

Lemma S4 (Freedman Inequality for Hermitian matrices, [43]) *Let $(\mathcal{F}_k)_k$ be a filtration, and let $(X_k)_k$ be a martingale difference sequence of d -dimensional Hermitian matrices such that $\|X_k\|_\infty \leq R$ for some $R > 0$. Then the partial sum $Y_k = \sum_{i=1}^k X_i$ and the predictable quadratic variation process $W_k = \sum_{i=1}^k \mathbb{E}[X_i^2 | \mathcal{F}_{i-1}]$ satisfies for all $t \geq 0$ and $\sigma^2 > 0$,*

$$\Pr(\exists k > 0 : \|Y_k\|_\infty > t \text{ and } \|W_k\|_\infty \leq \sigma^2) \leq 2d \exp\left(-\frac{t^2/2}{\sigma^2 + Rt/3}\right). \quad (\text{A.12})$$

Lemma S5 (Lattice-based random walk, [44]) *Consider a random walk $(\mathbf{x}^{(k)})_k$ on a lattice $\{-N, \dots, N\}^{\times L}$ with $\mathbf{x}^{(0)} = 0$, and there exists p_1, \dots, p_L such that for all j and k , $\Pr(\mathbf{x}^{(k)} - \mathbf{x}^{(k-1)} = \pm e_j) = p_j/2$. Then for any endpoint $\mathbf{x} \in \mathbb{Z}^L$ such that $\sum_j \mathbf{x}_j^2 = N$,*

$$\Pr_Q(\mathbf{x}^{(N)} = \mathbf{x}) = \frac{a_N(\mathbf{x})}{(2\pi N)^{L/2} \sqrt{\prod_{j=1}^L p_j}} \exp\left(-\frac{1}{2N} \sum_j \frac{\mathbf{x}_j^2}{p_j}\right) + o(N^{-L/2}), \quad (\text{A.13})$$

where a_N is the reachable parity function in Equation (A.1).

Appendix B: Thermal-drift channel

Let σ be an n -qubit Pauli operator and let $\tau \in \mathbb{R}_+$. We define the unnormalized imaginary-time evolution (ITE) maps at time τ in the two opposite directions by

$$\mathcal{E}_\sigma^\uparrow(\rho) = e^{-\tau\sigma/2} \rho e^{-\tau\sigma/2} \quad \text{and} \quad \mathcal{E}_\sigma^\downarrow(\rho) = e^{+\tau\sigma/2} \rho e^{+\tau\sigma/2}. \quad (\text{B.1})$$

Throughout this section, we use “ $\uparrow\downarrow$ ” to discuss both directions simultaneously. The goal is to construct a circuit that applies one of these two maps at random to an input state ρ on the main system and records the applied direction in an ancilla register.

To formalize this task, we introduce a $2n$ -qubit ancilla system AB and the n -qubit main system S . Based on the identity that

$$\text{Tr}[\mathcal{E}_\sigma^\uparrow(\rho) + \mathcal{E}_\sigma^\downarrow(\rho)] = \text{Tr}[(e^{-\tau\sigma} + e^{\tau\sigma})\rho] = (e^\tau + e^{-\tau}) \text{Tr}[\rho] = 2 \cosh(\tau), \quad (\text{B.2})$$

we define the thermal-drift channel $\mathcal{N}_\sigma(\rho) : \mathcal{D}(\mathcal{H}_S) \rightarrow \mathcal{D}(\mathcal{H}_{ABS})$ satisfying

$$\text{Tr}_{AB}[\Pi_{AB}^{\uparrow\downarrow} \mathcal{N}_\sigma(\rho)] = \frac{1}{2 \cosh(\tau)} \mathcal{E}_\sigma^{\uparrow\downarrow}(\rho), \quad (\text{B.3})$$

where Π^\pm are mutually orthogonal projectors on AB such that $\Pi^\uparrow + \Pi^\downarrow \prec I_{AB}$. Measuring the ancilla system AB in the projection-valued measure extending $\{\Pi^\uparrow, \Pi^\downarrow\}$ reveals which branch of Equation (B.3) occurred; the corresponding post-measurement state on S is obtained by tracing out AB and normalizing in the usual way.

The map satisfying Equation (B.3) is completely positive and trace-preserving under the chosen normalization, and thus admits a unitary dilation. The next theorem provides an explicit implementation with $\mathcal{O}(n)$ elementary gates, up to a heralded failure outcome Π° .

Theorem S6 *Suppose $\tau > 0$ and σ is an n -qubit Pauli operator that has no local identity term. Then there exists a projection-valued measure $\{\Pi^\uparrow, \Pi^\downarrow, \Pi^\circ\}$ on system AB , a τ -dependent ansatz U_τ and two fixed ansatzes T, V , such that the map $\mathcal{N}_\approx : \mathcal{D}(\mathcal{H}_S) \rightarrow \mathcal{D}(\mathcal{H}_{ABS})$ constructed in Figure S1 (dashed area) satisfies for all $\rho \in \mathcal{D}(\mathcal{H}_S)$,*

$$\text{Tr}_{AB}[\Pi_{AB}^\circ \mathcal{N}_\approx(\rho)] = p\rho \quad \text{and} \quad \text{Tr}_{AB}[\Pi_{AB}^{\uparrow\downarrow} \mathcal{N}_\approx(\rho)] = (1-p) \text{Tr}_{AB}[\Pi_{AB}^{\uparrow\downarrow} \mathcal{N}_\sigma(\rho)], \quad (\text{B.4})$$

where $p^{-1} = 2 \cosh^2(\tau/2)$, $\text{Tr}[\Pi^\uparrow] = \text{Tr}[\Pi^\downarrow]$ and \mathcal{N}_σ is given as in Equation (B.3). Moreover, implementation of \mathcal{N}_\approx takes $\mathcal{O}(n)$ single-qubit gates and CNOT gates; the projection-valued measure can be done in the computational basis.

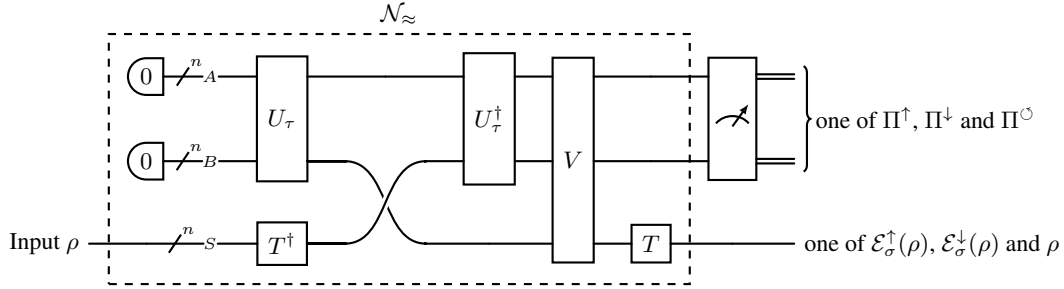


Fig S1. A circuit implementing the channel \mathcal{N}_\approx . Repeating \mathcal{N}_\approx and measuring AB in the computational basis until the outcome is not in Π° implements \mathcal{N}_σ .

Theorem S6 assumes that the Pauli operator has no local identity term; the next theorem removes this restriction and provides the resource bound for implementing a random-direction Pauli ITE step.

Theorem S7 *Suppose $\tau > 0$ and σ is an n -qubit Pauli operator. Then there exists a quantum channel $\mathcal{N}_\sigma : \mathcal{D}(\mathcal{H}_S) \rightarrow \mathcal{D}(\mathcal{H}_{ABS})$ and a measure-and-trace operation $\mathcal{M} : \mathcal{D}(\mathcal{H}_{ABS}) \rightarrow \{1, -1\} \times \mathcal{D}(\mathcal{H}_S)$ such that for all $\rho \in \mathcal{D}(\mathcal{H}_S)$,*

$$\mathcal{M} \circ \mathcal{N}_\sigma(\rho) = \begin{cases} (1, \mathcal{E}_\sigma^\uparrow(\rho) / \text{Tr}[e^{-\tau\sigma}\rho]), & \text{with probability } \text{Tr}[e^{-\tau\sigma}\rho] / (2 \cosh \tau); \\ (-1, \mathcal{E}_\sigma^\downarrow(\rho) / \text{Tr}[e^{\tau\sigma}\rho]), & \text{with probability } \text{Tr}[e^{\tau\sigma}\rho] / (2 \cosh \tau). \end{cases} \quad (\text{B.5})$$

Moreover, one can use $2n$ ancilla qubits and at most $\mathcal{O}(n \log(1/\delta))$ single-qubit gates and CNOT gates to implement \mathcal{N}_σ with probability at least $1 - \delta$; \mathcal{M} requires only computational-basis measurements and classical post-processing of the outcomes.

Proof We first consider the case where σ has no local identity term. Theorem S6 provides a projection-valued measure $\{\Pi^\uparrow, \Pi^\downarrow, \Pi^\circ\}$ and a channel \mathcal{N}_\approx such that

$$\mathrm{Tr}_{AB}[\Pi_{AB}^\circ \mathcal{N}_\approx(\rho)] = \frac{1}{2 \cosh^2(\tau/2)} \rho \quad \text{and} \quad \mathrm{Tr}_{AB}[\Pi_{AB}^{\uparrow\downarrow} \mathcal{N}_\approx(\rho)] = \left(1 - \frac{1}{2 \cosh^2(\tau/2)}\right) \mathrm{Tr}_{AB}[\Pi_{AB}^{\uparrow\downarrow} \mathcal{N}_\sigma(\rho)] \quad (\text{B.6})$$

Measuring $\mathcal{N}_\approx(\rho)$ on system AB with respect to $\{\Pi^\circ, I_{AB} - \Pi^\circ\}$ partitions the output into a fallback branch to ρ and a success branch to $\mathcal{N}_\sigma(\rho)$. Define \mathcal{M}_\circ to be the operation that measures AB and, upon obtaining Π° , traces out AB and outputs the remaining state on S ; define $\mathcal{M}_{\uparrow\downarrow}$ analogously for the complementary event $I_{AB} - \Pi^\circ$. For an integer $k \geq 1$, consider the repeat-until-success map

$$\mathcal{M}_{\uparrow\downarrow} \circ \mathcal{N}_\approx + \mathcal{M}_{\uparrow\downarrow} \circ \mathcal{N}_\approx \circ \mathcal{M}_\circ \circ \mathcal{N}_\approx + \dots + \mathcal{M}_{\uparrow\downarrow} \circ \mathcal{N}_\approx \circ (\mathcal{M}_\circ \circ \mathcal{N}_\approx)^{\circ k}. \quad (\text{B.7})$$

Since the fallback probability in each invocation is at most $1/2$, the probability of fallback in all $k+1$ attempts is at most $2^{-(k+1)}$. Choosing $k = \mathcal{O}(\log(1/\delta))$ ensures failure probability at most δ . Each invocation of \mathcal{N}_\approx uses $\mathcal{O}(n)$ elementary gates by Theorem S6, so the total gate count is $\mathcal{O}(n \log(1/\delta))$.

Conditioned on the success event $I_{AB} - \Pi^\circ$, the output is proportional to $\mathcal{N}_\sigma(\rho)$ as defined in Equation (B.3). We now define \mathcal{M} to measure AB with respect to $\{\Pi^\uparrow, \Pi^\downarrow\}$, trace out AB , and normalize the post-measurement state on S . Using $\mathrm{Tr}[\Pi^\uparrow] = \mathrm{Tr}[\Pi^\downarrow] = 2^{2n-2}$ and the fact that $\mathcal{E}_\sigma^\uparrow(\rho)$ and $\mathcal{E}_\sigma^\downarrow(\rho)$ have traces $\mathrm{Tr}[e^{-\tau\sigma}\rho]$ and $\mathrm{Tr}[e^{\tau\sigma}\rho]$, respectively, we obtain

$$\Pr(m=1) = \left(1 - \frac{1}{2 \cosh^2(\tau/2)}\right) \mathrm{Tr}[\Pi_{AB}^\uparrow \mathcal{N}_\sigma(\rho)] = \frac{\mathrm{Tr}[e^{-\tau\sigma}\rho]}{2 \cosh \tau}, \quad (\text{B.8})$$

$$\Pr(m=-1) = \left(1 - \frac{1}{2 \cosh^2(\tau/2)}\right) \mathrm{Tr}[\Pi_{AB}^\downarrow \mathcal{N}_\sigma(\rho)] = \frac{\mathrm{Tr}[e^{\tau\sigma}\rho]}{2 \cosh \tau}. \quad (\text{B.9})$$

Conditioning on each event yields the normalized post-measurement states $\mathcal{E}_\sigma^\uparrow(\rho)/\mathrm{Tr}[e^{-\tau\sigma}\rho]$ and $\mathcal{E}_\sigma^\downarrow(\rho)/\mathrm{Tr}[e^{\tau\sigma}\rho]$, as stated.

We now extend the construction to a general σ that may contain local identity terms. Let σ' be the tensor product of the non-identity local Pauli terms of σ , and let P be an n -qubit permutation gate such that $\sigma = P^\dagger(\sigma' \otimes I)P$. For any $\rho \in \mathcal{D}(\mathcal{H}_S)$,

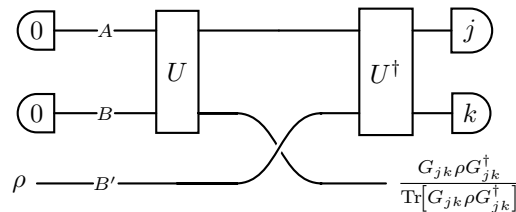
$$P^\dagger(\mathcal{E}_{\sigma'}^{\uparrow\downarrow} \otimes \mathbb{1})(P\rho P^\dagger)P = P^\dagger(e^{\mp\tau\sigma'/2} \otimes I)P \cdot \rho \cdot P^\dagger(e^{\mp\tau\sigma'/2} \otimes I)P \quad (\text{B.10})$$

$$= e^{\mp\tau\sigma/2} \rho e^{\mp\tau\sigma/2} = \mathcal{E}_\sigma^{\uparrow\downarrow}(\rho). \quad (\text{B.11})$$

Applying the above implementation to σ' (on the nontrivial subsystem) and conjugating by P therefore realizes the required instrument for σ . The permutation P can be implemented with at most $\mathcal{O}(n)$ CNOT gates, so the overall gate complexity remains $\mathcal{O}(n \log(1/\delta))$. ■

The remainder of this section proves Theorem S6 by explicitly constructing U_τ , T , and V . We start from a SWAP-based construction that realizes a family of Kraus operators from a unitary on a larger space.

Lemma S8 *Suppose U is a unitary acting on a bipartite system AB . Then for $G_{jk} = \mathrm{Tr}_A[U|00\rangle\langle jk|U^\dagger]$ and an additional system B' such that $|B'| = |B|$, the following circuit of systems ABB' holds*



Proof Let $U = \sum_{x,y,z,t} C_{xyzt} |xy\rangle\langle zt|$ and $\text{SWAP} = \sum_{l,m} |lm\rangle\langle ml|$. For the operator acting on B' conditioned on outcomes (j,k) on AB , we compute

$$(\langle j_A j_B | U^\dagger \rangle_{AB} \text{SWAP}_{BB'} (U |k_A k_B \rangle)_{AB})_{AB} \quad (\text{B.12})$$

$$= \sum_{x,y,z,t,m,l} C_{j_A j_B z t}^* C_{x y k_A k_B} (\langle z|_A \otimes \langle t|_B) (|l\rangle\langle m|_B \otimes |m\rangle\langle l|_{B'}) (|x\rangle_A \otimes |y\rangle_B) \quad (\text{B.13})$$

$$= \sum_{x,y,z,t,m,l} C_{j_A j_B z t}^* C_{x y k_A k_B} \delta_{z,x} \delta_{t,l} \delta_{m,y} |m\rangle \langle l|_{B'} \quad (\text{B.14})$$

$$= \sum_{x,y,z,t} C_{j_A j_B z t}^* C_{x y k_A k_B} \delta_{z,x} |y\rangle \langle t| \quad (\text{B.15})$$

$$= \text{Tr}_A \left[\sum_{x,y,z,t} C_{j_A j_B z t}^* C_{x y k_A k_B} |x y\rangle \langle z t|_{AB} \right] = \text{Tr}_A [U |k_A k_B\rangle \langle j_A j_B| U^\dagger]. \quad (\text{B.16})$$

For any pure state $|\psi\rangle$ on B' , substituting this identity into the circuit shows that

$$U_{AB}^\dagger \text{SWAP}_{BB'} U_{AB} (|00\rangle \otimes |\psi\rangle) = \sum_{j,k} |jk\rangle \langle jk|_{AB} U_{AB}^\dagger \text{SWAP}_{BB'} U_{AB} (|00\rangle \otimes |\psi\rangle) \quad (\text{B.17})$$

$$= \sum_{j,k} |jk\rangle_{AB} (\langle jk| U^\dagger)_{AB} \text{SWAP}_{BB'} (U|00\rangle)_{AB} |\psi\rangle_{B'} \quad (\text{B.18})$$

$$= \sum_{j,k} |jk\rangle_{AB} G_{jk} |\psi\rangle_{B'} = \sum_{j,k} |jk\rangle \otimes G_{jk} |\psi\rangle. \quad (\text{B.19})$$

When the system AB is measured to be jk , the unnormalized post-measurement state on B' is $G_{jk} |\psi\rangle$, and hence the normalized post-measurement state is $G_{jk} |\psi\rangle / \|G_{jk} |\psi\rangle\|$. By linearity, the same conclusion holds for a mixed input ρ , yielding the claimed output state $G_{jk} \rho G_{jk}^\dagger / \text{Tr} [G_{jk} \rho G_{jk}^\dagger]$. \blacksquare

We now prove Theorem S6. All three systems A, B, S are n -qubit. In the following analysis, A_i denotes the i -th qubit in system A (counting from top to bottom), and similarly for B and S .

Theorem S6 (Complete version) *Suppose $\tau > 0$ and σ is an n -qubit Pauli operator that has no local identity term. Consider the following construction of a projection-valued measure on the system AB ,*

$$\Pi^\circ = |1\rangle \langle 1|_{A_n}, \quad \Pi^\uparrow = |0\rangle \langle 0|_{A_n} \otimes |0\rangle \langle 0|_{B_n}, \quad \Pi^\downarrow = |0\rangle \langle 0|_{A_n} \otimes |1\rangle \langle 1|_{B_n}, \quad (\text{B.20})$$

and of circuit ansatzes on system ABS ,

$$U_\tau = \left(\prod_{i=1}^n \text{CNOT}_{A_i B_i} \right) \left(\prod_{i=1}^{n-1} \text{CNOT}_{A_i A_n} \right) \left(H^{\otimes(n-1)} \otimes R_y(2\theta) \right)_A, \quad (\text{B.21})$$

$$V = \left(\prod_{i=1}^n \text{CNOT}_{B_i B_n} \right) \left(\prod_{i=1}^n \text{CNOT}_{B_i S_i} \text{CZ}_{A_i S_i} \right) \left(\prod_{i=1}^{n-1} \text{CNOT}_{A_n A_i} \right), \quad (\text{B.22})$$

$$T \text{ satisfies } T Z^{\otimes n} T^\dagger = \sigma, \quad (\text{B.23})$$

where $\theta = \arccos \sqrt{e^{-\tau/2} / (2 \cosh(\tau/2))}$. Then the map \mathcal{N}_\approx constructed in Figure S1 (dashed area) satisfies

$$\text{Tr}_{AB} [\Pi_{AB}^\circ \mathcal{N}_\approx(\rho)] = \frac{1}{2 \cosh^2(\tau/2)} \rho \quad \text{and} \quad \text{Tr}_{AB} [\Pi_{AB}^{\uparrow\downarrow} \mathcal{N}_\approx(\rho)] = \frac{1}{4 \cosh^2(\tau/2)} \mathcal{E}_\sigma^{\uparrow\downarrow}(\rho). \quad (\text{B.24})$$

Proof The proof is decomposed into two parts: we first **(1)** analyze what G_{jk} is by taking U_τ into Lemma S8, and show that **(2)** V can decode, map and group these G_{jk} to be either $e^{-\tau\sigma/2}$, $e^{\tau\sigma/2}$ or the identity matrix. Taking the whole picture gives the statement.

(1) For the first part, one can derive that for all $|j\rangle = |j_1 \cdots j_n\rangle$ in system A ,

$$\left(\prod_{i=1}^{n-1} \text{CNOT}_{A_i A_n} \right) \left(H^{\otimes(n-1)} \otimes R_y(2\theta) \right) |j\rangle \quad (\text{B.25})$$

$$= \left(\prod_{i=1}^{n-1} \text{CNOT}_{A_i A_n} \right) \left(H^{\otimes(n-1)} |j_{1:n}\rangle \otimes R_y(2\theta) |j_n\rangle \right) \quad (\text{B.26})$$

$$= \frac{1}{\sqrt{2^{n-1}}} \left(\prod_{i=1}^{n-1} \text{CNOT}_{A_i A_n} \right) \sum_{x \in \{0,1\}^{n-1}} (-1)^{x \cdot j_{1:n}} |x\rangle \otimes (\cos(\theta) |j_n\rangle + (-1)^{j_n} \sin(\theta) X |j_n\rangle) \quad (\text{B.27})$$

$$= \frac{1}{\sqrt{2^{n-1}}} \sum_{x \in \{0,1\}^{n-1}} (-1)^{x \cdot j_{1:n}} |x\rangle \otimes \left(\cos(\theta) |j_n \oplus p(x)\rangle + (-1)^{j_n} \sin(\theta) |j_n \oplus p(x) \oplus 1\rangle \right), \quad (\text{B.28})$$

where $j_{1:n} = j_1 \cdots j_{n-1}$, \oplus is the bitwise addition and $p(x)$ is the bitwise parity function defined in Equation (A.2). Taking the last piece of U_τ gives

$$U_\tau |jk\rangle = \left(\prod_{i=1}^n \text{CNOT}_{A_i B_i} \right) \left(\prod_{i=1}^{n-1} \text{CNOT}_{A_i A_n} \right) \left(H^{\otimes(n-1)} \otimes R_y(2\theta) \right) (|j\rangle_A \otimes |k\rangle_B) \quad (\text{B.29})$$

$$= \left(\prod_{i=1}^n \text{CNOT}_{A_i B_i} \right) \frac{1}{\sqrt{2^{n-1}}} \sum_{x \in \{0,1\}^{n-1}} (-1)^{x \cdot j_{1:n}} |x\rangle_{A_{1:n}} \otimes \left(\cos(\theta) |j'_n\rangle_{A_n} + (-1)^{j_n} \sin(\theta) |j'_n \oplus 1\rangle_{A_n} \right) \otimes |k\rangle_B \quad (\text{B.30})$$

$$= \sum_{x \in \{0,1\}^{n-1}} \frac{(-1)^{x \cdot j_{1:n}}}{\sqrt{2^{n-1}}} |x\rangle_{A_{1:n}} |k_{1:n} \oplus x\rangle_{B_{1:n}} \left(\cos(\theta) |j'_n\rangle_{A_n} |k'_n\rangle_{B_n} + (-1)^{j_n} \sin(\theta) |j'_n \oplus 1\rangle_{A_n} |k'_n \oplus 1\rangle_{B_n} \right) \quad (\text{B.31})$$

for $j'_n = j_n \oplus p(x)$ and $k'_n = k_n \oplus j'_n$. When j and k are both zero, we have

$$U_\tau |00\rangle = \frac{1}{\sqrt{2^{n-1}}} \sum_{x \in \{0,1\}^{n-1}} |x\rangle_{A_{1:n}} |x\rangle_{B_{1:n}} \left(\cos(\theta) |p(x)\rangle_{A_n} |p(x)\rangle_{B_n} + \sin(\theta) |p(x) \oplus 1\rangle_{A_n} |p(x) \oplus 1\rangle_{B_n} \right). \quad (\text{B.32})$$

Then we have

$$U_\tau |00\rangle \langle jk | U_\tau^\dagger = \frac{1}{2^{n-1}} \sum_{x \in \{0,1\}^{n-1}} (-1)^{x \cdot j_{1:n}} |x\rangle \langle x|_{A_{1:n}} |x\rangle \langle k_{1:n} \oplus x|_{B_{1:n}}. \quad (\text{B.33})$$

$$\left(\cos(\theta) |p(x)\rangle_{A_n} \langle p(x)|_{B_n} + \sin(\theta) |p(x) \oplus 1\rangle_{A_n} \langle p(x) \oplus 1|_{B_n} \right). \quad (\text{B.34})$$

$$\left(\cos(\theta) \langle j'_n |_{A_n} \langle k'_n |_{B_n} + (-1)^{j_n} \sin(\theta) \langle j'_n \oplus 1 |_{A_n} \langle k'_n \oplus 1 |_{B_n} \right). \quad (\text{B.35})$$

G_{jk} in Lemma S8 is given as

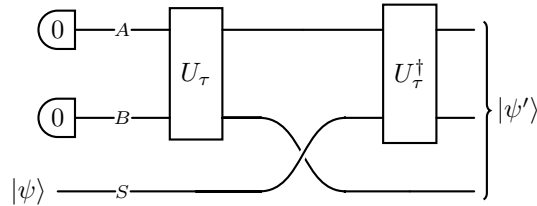
$$G_{jk} = \text{Tr}_A [U_\tau |00\rangle \langle jk | U_\tau^\dagger] = \frac{1}{2^{n-1}} \sum_{x \in \{0,1\}^{n-1}} (-1)^{x \cdot j_{1:n}} |x\rangle \langle k_{1:n} \oplus x| \otimes Q_{j_n k_n}, \quad (\text{B.36})$$

where $Q_{j_n k_n}$ is constructed as

$$Q_{j_n k_n} = \delta_{p(x), j'_n} \left(\cos^2(\theta) |p(x)\rangle \langle k'_n| + (-1)^{j_n} \sin^2(\theta) X |p(x)\rangle \langle k'_n| X \right) + \quad (\text{B.37})$$

$$\frac{1}{2} \delta_{p(x), (j'_n \oplus 1)} \sin(2\theta) \left(X |p(x)\rangle \langle k'_n| + (-1)^{j_n} |p(x)\rangle \langle k'_n| X \right). \quad (\text{B.38})$$

(2) For the second part, without loss of generality, suppose $\rho = |\psi\rangle \langle \psi|$ is a pure state. At this point, by Lemma S8, the output state $|\psi'\rangle$ of the following circuit



can be expressed as $|\psi'\rangle = \sum_{j,k} |jk\rangle \otimes G_{jk} |\psi\rangle$. Then

$$V |\psi'\rangle = \left(\prod_{i=1}^n \text{CNOT}_{B_i B_n} \right) \left(\prod_{i=1}^n \text{CNOT}_{B_i S_i} \text{CZ}_{A_i S_i} \right) \left(\prod_{i=1}^{n-1} \text{CNOT}_{A_n A_i} \right) \sum_{j,k} |j\rangle \otimes |k\rangle \otimes G_{jk} |\psi\rangle \quad (\text{B.39})$$

$$= \left(\prod_{i=1}^n \text{CNOT}_{B_i B_n} \right) \left(\prod_{i=1}^n \text{CNOT}_{B_i S_i} \text{CZ}_{A_i S_i} \right) \sum_{j,k} \left(\bigotimes_{i=1}^{n-1} |j_i \oplus j_n\rangle \right) \otimes |j_n\rangle \otimes |k\rangle \otimes G_{jk} |\psi\rangle \quad (\text{B.40})$$

$$= \left(\prod_{i=1}^n \text{CNOT}_{B_i B_n} \right) \left(\prod_{i=1}^n \text{CNOT}_{B_i S_i} \right) \left(\prod_{i=1}^n \text{CZ}_{A_i S_i} \right) \sum_{j,k} \left(\bigotimes_{i=1}^{n-1} |j_i \oplus j_n\rangle \right) \otimes |j_n\rangle \otimes |k\rangle \otimes G_{jk} |\psi\rangle \quad (\text{B.41})$$

$$= \left(\prod_{i=1}^n \text{CNOT}_{B_i B_n} \right) \sum_{j,k} \left(\bigotimes_{i=1}^{n-1} |j_i \oplus j_n\rangle \right) \otimes |j_n\rangle \otimes |k\rangle \otimes E_{jk} |\psi\rangle \quad (\text{B.42})$$

$$= \sum_{j,k} \left(\bigotimes_{i=1}^{n-1} |j_i \oplus j_n\rangle \right) \otimes |j_n\rangle \otimes |k_{1:n}\rangle \otimes |p(k)\rangle \otimes E_{jk} |\psi\rangle \quad (\text{B.43})$$

for E_{jk} constructed as

$$E_{jk} = X^{(k)} \left(\prod_{i=1}^{n-1} Z_{S_i}^{j_i + j_n} \right) Z_{S_n}^{j_n} G_{jk}, \quad (\text{B.44})$$

where $X^{(k)}$ is short for $\bigotimes_{i=1}^n X^{k_i}$. Now we analyze what E_{jk} will be for three cases: $j_n = 1$, $(j_n, p(k)) = (0, 0)$ and $(j_n, p(k)) = (0, 1)$.

If $j_n = 1$, then $j'_n = j_n \oplus p(x) = p(x) \oplus 1$, $k'_n = k_n \oplus j'_n = k_n \oplus p(x) \oplus 1$ and $Q_{j_n k_n}$ in Equation (B.37) satisfies

$$Q_{j_n k_n} = \frac{1}{2} \sin(2\theta) (X|p(x)\rangle\langle k_n \oplus p(x)|X - |p(x)\rangle\langle k_n \oplus p(x)|) \quad (\text{B.45})$$

and hence

$$G_{jk} = \frac{1}{2^n} \sin(2\theta) \sum_{x \in \{0,1\}^{n-1}} (-1)^{x \cdot j_{1:n}} |x\rangle\langle k_{1:n} \oplus x| \otimes (X|p(x)\rangle\langle k_n \oplus p(x)|X - |p(x)\rangle\langle k_n \oplus p(x)|) \quad (\text{B.46})$$

and hence

$$E_{jk} = \frac{\sin(2\theta)}{2^n} X^{(k)} \left(\prod_{i=1}^{n-1} Z_{S_i}^{j_i + 1} \right) Z_{S_n} \sum_{x \in \{0,1\}^{n-1}} (-1)^{x \cdot j_{1:n}} |x\rangle\langle k_{1:n} \oplus x| \otimes (X|p(x)\rangle\langle k_n \oplus p(x)|X - |p(x)\rangle\langle k_n \oplus p(x)|) \quad (\text{B.47})$$

$$= \frac{\sin(2\theta)}{2^n} X^{(k)} \sum_{x \in \{0,1\}^{n-1}} (-1)^x |x\rangle\langle k_{1:n} \oplus x| \otimes \left((-1)^{p(x)+1} |p(x) \oplus 1\rangle\langle k_n \oplus p(x) \oplus 1| - (-1)^{p(x)} |p(x)\rangle\langle k_n \oplus p(x)| \right) \quad (\text{B.48})$$

$$= \frac{\sin(2\theta)}{2^n} \sum_{x \in \{0,1\}^{n-1}} (-1)^x |x \oplus k_{1:n}\rangle\langle k_{1:n} \oplus x| \otimes (-1)^{p(x)+1} (|p(x) \oplus k_n \oplus 1\rangle\langle k_n \oplus p(x) \oplus 1| + |p(x) \oplus k_n\rangle\langle k_n \oplus p(x)|) \quad (\text{B.49})$$

$$= -\frac{\sin(2\theta)}{2^n} \sum_{x \in \{0,1\}^{n-1}} |x \oplus k_{1:n}\rangle\langle k_{1:n} \oplus x| \otimes I = -\frac{1}{2^n} \sin(2\theta) I_S. \quad (\text{B.50})$$

If $j_n = 0$, then $j'_n = j_n \oplus p(x) = p(x)$, $k'_n = k_n \oplus j'_n = k_n \oplus p(x)$ and hence

$$Q_{j_n k_n} = \cos^2(\theta) |p(x)\rangle\langle k_n \oplus p(x)| + \sin^2(\theta) X|p(x)\rangle\langle k_n \oplus p(x)|X \quad (\text{B.51})$$

$$\implies G_{jk} = \frac{1}{2^{n-1}} \sum_{x \in \{0,1\}^{n-1}} (-1)^{x \cdot j_{1:n}} |x\rangle\langle k_{1:n} \oplus x| \otimes (\cos^2(\theta) |p(x)\rangle\langle k_n \oplus p(x)| + \sin^2(\theta) X|p(x)\rangle\langle k_n \oplus p(x)|X), \quad (\text{B.52})$$

which gives

$$E_{jk} = X^{(k)} Z_{S_{1:n}}^{(j_{1:n})} G_{jk} \quad (\text{B.53})$$

$$= \frac{1}{2^{n-1}} X^{(k)} \sum_{x \in \{0,1\}^{n-1}} |x\rangle\langle k_{1:n} \oplus x| \otimes (\cos^2(\theta)|p(x)\rangle\langle k_n \oplus p(x)| + \sin^2(\theta)X|p(x)\rangle\langle k_n \oplus p(x)|X) \quad (\text{B.54})$$

$$= \frac{1}{2^{n-1}} X^{(k)} \left[\sum_{x \in \{0,1\}^{n-1}} |x\rangle\langle x| \otimes (\cos^2(\theta)|p(x)\rangle\langle p(x)| + \sin^2(\theta)X|p(x)\rangle\langle p(x)|X) \right] X^{(k)}. \quad (\text{B.55})$$

Denote $C = 2 \cosh(\tau/2) = e^{-\tau/2} + e^{\tau/2}$. Since $\cos^2(\theta) = e^{-\tau/2}/C$ and $\sin^2(\theta) = e^{\tau/2}/C$, the expression surrounded by the square bracket is simplified as

$$\sum_{x \in \{0,1\}^{n-1}} |x\rangle\langle x| \otimes (\cos^2(\theta)|p(x)\rangle\langle p(x)| + \sin^2(\theta)X|p(x)\rangle\langle p(x)|X) \quad (\text{B.56})$$

$$= \frac{1}{C} \sum_{x \in \{0,1\}^{n-1}} |x\rangle\langle x| \otimes (e^{-\tau/2}|p(x)\rangle\langle p(x)| + e^{\tau/2}|p(x) \oplus 1\rangle\langle p(x) \oplus 1|) \quad (\text{B.57})$$

$$= \frac{1}{C} \sum_{x \in \{0,1\}^{n-1}} |x\rangle\langle x| \otimes \exp(-\frac{\tau}{2}(-1)^{p(x)}Z) = \frac{1}{C} e^{-\tau Z^{\otimes n}/2}, \quad (\text{B.58})$$

where the last equality comes from the fact that $Z^{\otimes(n-1)}|x\rangle = (-1)^{p(x)}|x\rangle$. Then

$$E_{jk} = \frac{1}{2^{n-1}C} X^{(k)} e^{-\tau Z^{\otimes n}/2} X^{(k)} \quad (\text{B.59})$$

$$= \frac{1}{2^{n-1}C} \begin{cases} e^{-\tau Z^{\otimes n}/2}, & \text{if } p(k) = 0, \\ e^{\tau Z^{\otimes n}/2}, & \text{if } p(k) = 1. \end{cases} \quad (\text{B.60})$$

As a result, omitting subsystems $A_{1:n}$ and $B_{1:n}$, since $TZ^{\otimes n}T^\dagger = \sigma$, we have

$$T_S V T_S^\dagger |\psi'\rangle = \sum_{j,k} \dots \otimes |j_n\rangle_{A_n} \otimes |p(k)\rangle_{B_n} \otimes T E_{jk} T^\dagger |\psi\rangle \quad (\text{B.61})$$

$$= - \sum_{j_n=1} \dots \otimes |1\rangle_{A_n} \otimes |p(k)\rangle_{B_n} \otimes \frac{1}{2^n} \sin(2\theta) |\psi\rangle + \quad (\text{B.62})$$

$$\sum_{(j_n, p(k))=(0,0)} \dots \otimes |0\rangle_{A_n} \otimes |0\rangle_{B_n} \otimes \frac{1}{2^{n-1}C} e^{-\tau\sigma/2} |\psi\rangle + \quad (\text{B.63})$$

$$\sum_{(j_n, p(k))=(0,1)} \dots \otimes |0\rangle_{A_n} \otimes |1\rangle_{B_n} \otimes \frac{1}{2^{n-1}C} e^{\tau\sigma/2} |\psi\rangle. \quad (\text{B.64})$$

There are 2^{2n-1} , 2^{2n-2} , 2^{2n-2} pairs of (j, k) for satisfying $j_n = 1$, $(j_n, p(k)) = (0, 0)$ and $(j_n, p(k)) = (0, 1)$, respectively. Finally, taking $\Pi^\circ, \Pi^\uparrow, \Pi^\downarrow$ in Equation (B.20) gives

$$\text{Tr}_{AB} [\Pi_{AB}^\circ \mathcal{N}_{\approx}(|\psi\rangle\langle\psi|)] = 2^{2n-1} \cdot \frac{1}{2^{2n}} \sin^2(2\theta) |\psi\rangle\langle\psi| = \frac{1}{2 \cosh^2(\tau/2)} |\psi\rangle\langle\psi|, \quad (\text{B.65})$$

$$\text{Tr}_{AB} [\Pi_{AB}^\uparrow \mathcal{N}_{\approx}(|\psi\rangle\langle\psi|)] = 2^{2n-2} \cdot \frac{1}{2^{2n-2} C^2} e^{-\tau\sigma/2} |\psi\rangle\langle\psi| e^{-\tau\sigma/2} = \frac{1}{4 \cosh^2(\tau/2)} \mathcal{E}_\sigma^\uparrow(|\psi\rangle\langle\psi|), \quad (\text{B.66})$$

$$\text{Tr}_{AB} [\Pi_{AB}^\downarrow \mathcal{N}_{\approx}(|\psi\rangle\langle\psi|)] = 2^{2n-2} \cdot \frac{1}{2^{2n-2} C^2} e^{\tau\sigma/2} |\psi\rangle\langle\psi| e^{\tau\sigma/2} = \frac{1}{4 \cosh^2(\tau/2)} \mathcal{E}_\sigma^\downarrow(|\psi\rangle\langle\psi|). \quad (\text{B.67})$$

The statement holds by generalizing $|\psi\rangle\langle\psi|$ to ρ by linearity. ■

Appendix C: Sampling thermal states and their labels

Let $\beta > 0$ and let $\Sigma = \{\sigma_j\}_{j=1}^L$ be a set of L n -qubit Pauli operators with a boundary vector $h \in \mathbb{R}_+^L$. The goal of random thermal state generation is to sample a datum $(G_{\beta, H}, H)$ from the dataset

$$S(\beta, \Sigma, h) = \left\{ (G_{\beta, H}, H) : H = \sum_{j=1}^L c_j \sigma_j, |c_j| \leq h_j, c_j \in \mathbb{R}, \sigma_j \in \Sigma \right\} \quad (\text{C.1})$$

where $G_{\beta,H} = e^{-\beta H} / \text{Tr}[e^{-\beta H}]$ is the thermal state of the Hamiltonian H at temperature β^{-1} . To avoid sampling continuous coefficients directly, we sample from a quantized surrogate. For $N \geq 1$ define

$$S_N(\beta, \Sigma, h) = \left\{ (G_{\beta,H}, H) : H = \sum_{j=1}^L c_j \sigma_j, |c_j| \leq h_j, c_j/h_j \in (1/N)\mathbb{Z}, \sigma_j \in \Sigma \right\} \quad (\text{C.2})$$

so that $\bigcup_{N \geq 1} S_N(\beta, \Sigma, h)$ is dense in $S(\beta, \Sigma, h)$ with respect to the sup-norm on the coefficient vector. The following algorithm describes how to sample a data from $S_N(\beta, \Sigma, h)$.

Algorithm 1: Pseudo code for our thermal state sampler

Input : Inverse temperature β , a set Σ of n -qubit Pauli operators with a boundary vector h , a number of steps N

Output: A datum $(G_{\beta,H}, H) \in S_N(\beta, \Sigma, h)$

- 1 $\tau \leftarrow \lambda\beta/N, \rho \leftarrow I^{\otimes n}/2^n;$
 - 2 SAMPLE \leftarrow a classical function that returns a value j with weight $p_j = h_j/\lambda;$
 - 3 **for** $k = 1, \dots, N$ **do**
 - 4 $j_k \leftarrow \text{SAMPLE}();$
 - 5 $\mathcal{M}_{j_k}, \mathcal{N}_{\sigma_{j_k}} \leftarrow \text{Theorem S7 wrt. } \sigma_{j_k}.$
 - 6 $(m_k, \rho) \leftarrow (\mathcal{M}_{j_k} \circ \mathcal{N}_{\sigma_{j_k}})(\rho);$
 - 7 $c_j \leftarrow \lambda \sum_{k: j_k=j} m_k/N, H \leftarrow \sum_{j=1}^L c_j \sigma_j;$
 - 8 **return** (H, ρ)
-

This section develops two technical components used to analyze Algorithm 1. First, we prove the trace-norm error bound between the algorithmic output state and the target thermal state (Theorem 1). Second, we set up the random-walk viewpoint for the induced Hamiltonian coefficients, which underlies the sampling-probability analysis in Theorem 2.

1. Error analysis

Fix the step number N and a sequence of indices $(j_k)_{k=1}^N \subset [L]$ selecting Pauli operators from $\Sigma = \{\sigma_j\}_{j=1}^L$, as in Algorithm 1. Let ρ_k denote the (normalized) system state after k steps, and define the step size $\tau = \lambda\beta/N$. Then $(\rho_k)_{k=0}^N$ evolves according to the Markovian update rule

$$\rho_0 = I/2^n, \quad \rho_k = \mathcal{M}_{j_k} \circ \mathcal{N}_{j_k}(\rho_{k-1}) = \frac{e^{B_k} \rho_{k-1} e^{B_k}}{\text{Tr}[e^{B_k} \rho_{k-1} e^{B_k}]}, \quad (\text{C.3})$$

where $\mathcal{M}_{j_k}, \mathcal{N}_{j_k}$ are specified by Theorem S7 for σ_{j_k} . The corresponding random variable B_k takes the form

$$B_k = \begin{cases} \tau\sigma_{j_k}/2, & \text{with probability } \text{Tr}[e^{\tau\sigma_{j_k}} \rho_{k-1}]/2 \cosh \tau, \\ -\tau\sigma_{j_k}/2, & \text{with probability } \text{Tr}[e^{-\tau\sigma_{j_k}} \rho_{k-1}]/2 \cosh \tau. \end{cases} \quad (\text{C.4})$$

Iterating Equation (C.3) shows that the final output state can be written as

$$\rho_N = \frac{(\prod_{k=N}^1 e^{B_k}) \rho_0 (\prod_{k=1}^N e^{B_k})}{\text{Tr}[\text{same above}]} = \frac{(\prod_{k=N}^2 e^{B_k}) e^{2B_1} (\prod_{k=2}^N e^{B_k})}{\text{Tr}[\text{same above}]}, \quad (\text{C.5})$$

where $\prod_{k=N}^2$ denotes the ordered product from N down to 2. The corresponding target thermal state is

$$G_{\beta,H} = \frac{e^{-\beta H}}{\text{Tr}[e^{-\beta H}]} \quad \text{for} \quad H = -\frac{2}{\beta} \sum_{k=1}^N B_k. \quad (\text{C.6})$$

In this subsection, we prove Theorem 1, which shows that, with probability at least $1 - \delta$ and for sufficiently large N ,

$$\|\rho_N - G_{\beta,H}\|_1 \leq \mathcal{O}\left((n + \log(N/\delta))^{3/2} \lambda^3 \beta^3 N^{-3/2}\right). \quad (\text{C.7})$$

Two lemmas simplify the proof. The first lemma compares the palindromic product in ρ_N with the exponential of the accumulated generator.

Lemma S10 Let $(B_k)_{k=1}^N$ be a sequence of matrices. Denote $S_k = \sum_{j=1}^k B_j$. Suppose $\max_{1 \leq j \leq N} \|B_j\|_\infty = \tau \ll 1$. Then

$$\log \left(\left(\prod_{j=N}^2 e^{B_j} \right) e^{2B_1} \left(\prod_{j=2}^N e^{B_j} \right) \right) = 2S_N + \Delta_N + \mathcal{R}_N, \quad (\text{C.8})$$

where $\Delta_k = -\frac{1}{6} \sum_{j=2}^k [B_j + 2S_{j-1}, [B_j, 2S_{j-1}]]$ denotes the terms of order 3 and \mathcal{R}_N denotes the remainder terms. We have

$$\|\mathcal{R}_N\|_\infty = \mathcal{O} \left(\sum_{r=5, r \text{ is odd}}^{\infty} \frac{1}{r!} \sum_{k=2}^N \|\text{ad}_{2S_{k-1}}^{r-1}(B_k)\|_\infty \right). \quad (\text{C.9})$$

Proof For Hermitian X and Y , since $(e^X e^Y e^X)^{-1} = e^{-X} e^{-Y} e^{-X}$, we have

$$\log(e^X e^Y e^X) + \log(e^{-X} e^{-Y} e^{-X}) = 0, \quad (\text{C.10})$$

which implies $f(X, Y) = \log(e^X e^Y e^X) = -f(-X, -Y)$. Hence, the BCH expansion of $\log(e^X e^Y e^X)$ contains no even-order terms.

We proceed by induction using the palindromic products

$$M_k := \left(\prod_{j=k}^2 e^{B_j} \right) e^{2B_1} \left(\prod_{j=2}^k e^{B_j} \right), \quad Z_k := \log(M_k). \quad (\text{C.11})$$

We have $M_1 = e^{2B_1}$, and for $k \geq 2$, $M_k = e^{B_k} M_{k-1} e^{B_k} = e^{B_k} e^{Z_{k-1}} e^{B_k}$.

For $k = 1$, we have $Z_1 = \log(e^{2B_1}) = 2B_1 = 2S_1$, so the claim holds.

Now fix $k \geq 2$ and assume inductively that $Z_{k-1} = 2S_{k-1} + \Delta_{k-1} + \mathcal{R}_{k-1}$, where Δ_{k-1} collects the cubic terms and \mathcal{R}_{k-1} collects the remaining odd-order terms of degree at least 5. Applying Lemma S3 to $e^{B_k} e^{Z_{k-1}} e^{B_k}$ gives

$$Z_k = \log(e^{B_k} e^{Z_{k-1}} e^{B_k}) \quad (\text{C.12})$$

$$= \log(e^{B_k} e^{2S_{k-1} + \Delta_{k-1} + \mathcal{R}_{k-1}} e^{B_k}) \quad (\text{C.13})$$

$$= 2S_k + \Delta_{k-1} + \mathcal{R}_{k-1} - \frac{1}{6} [B_k + 2S_{k-1} + \Delta_{k-1} + \mathcal{R}_{k-1}, [B_k, 2S_{k-1} + \Delta_{k-1} + \mathcal{R}_{k-1}]]. \quad (\text{C.14})$$

Separating the cubic contribution from higher-order terms yields

$$\Delta_k = \Delta_{k-1} - \frac{1}{6} [B_k + 2S_{k-1}, [B_k, 2S_{k-1}]], \quad (\text{C.15})$$

$$\mathcal{R}_k = \mathcal{R}_{k-1} - \frac{1}{6} [B_k + 2S_{k-1}, [B_k, \Delta_{k-1} + \mathcal{R}_{k-1}]] - \frac{1}{6} [\Delta_{k-1} + \mathcal{R}_{k-1}, [B_k, 2S_{k-1} + \Delta_{k-1} + \mathcal{R}_{k-1}]]. \quad (\text{C.16})$$

Iterating the recursion for Δ_k gives

$$\Delta_N = \Delta_{N-1} - \frac{1}{6} [B_N + 2S_{N-1}, [B_N, 2S_{N-1}]] \quad (\text{C.17})$$

$$= -\frac{1}{6} \sum_{k=2}^N [B_k + 2S_{k-1}, [B_k, 2S_{k-1}]]. \quad (\text{C.18})$$

It remains to bound the remainder terms in \mathcal{R}_N . Write $\mathcal{R}_k = \sum_{r \geq 5, r \text{ odd}} \mathcal{R}_{k,r}$, where $\mathcal{R}_{k,r}$ denotes the homogeneous terms of total order r , and assume $\|B_k\|_\infty = \mathcal{O}(\|S_{k-1}\|_\infty)$ for $k \geq 2$. From the recursive definition of \mathcal{R}_k , the order- r component obeys

$$\mathcal{R}_{k,r} = \mathcal{R}_{k-1,r} + \frac{1}{6} [B_k + 2S_{k-1}, [\mathcal{R}_{k-1,r-2}, B_k]] + \frac{1}{6} \sum_{j=3}^{r-4} [\mathcal{R}_{k-1,j}, [\mathcal{R}_{k-1,r-1-j}, B_k]]. \quad (\text{C.19})$$

We claim that, for each odd $r \geq 5$, the increment $\mathcal{R}_{k,r} - \mathcal{R}_{k-1,r}$ is dominated (up to constants depending only on r) by terms of the form $\text{ad}_{2S_{k-1}}^{r-1}(B_k)$. The claim is immediate for $r = 5$, and the recursion preserves the dominance for higher odd orders.

Finally, since the coefficient of $\text{ad}_X^{r-1}(Y)$ in the BCH expansion of $\log(e^X e^Y e^X)$ has magnitude $2/r!$, there exists a constant C_r (depending only on r) such that, for all odd $r \geq 5$,

$$\|\mathcal{R}_{N,r}\|_\infty \leq \frac{C_r}{r!} \sum_{k=2}^N \|\text{ad}_{2S_{k-1}}^{r-1}(B_k)\|_\infty. \quad (\text{C.20})$$

Summing over odd $r \geq 5$ gives the stated bound on $\|\mathcal{R}_N\|_\infty$. \blacksquare

The second lemma controls the effect of normalizing matrix exponentials.

Lemma S11 *Let A, E be two Hermitian matrices. Then*

$$\left\| \frac{e^{A+E}}{\text{Tr}[e^{A+E}]} - \frac{e^A}{\text{Tr}[e^A]} \right\|_1 \leq 2\|E\|_\infty. \quad (\text{C.21})$$

Proof Consider $t \in [0, 1]$, $A(t) = A + tE$ and $\rho(t) = e^{A(t)}/\mathcal{Z}(t)$ with $\mathcal{Z}(t) = \text{Tr}[e^{A(t)}]$. By Lemma S1, we have

$$\frac{d}{dt} e^{A(t)} = \int_0^1 e^{sA(t)} E e^{(1-s)A(t)} ds. \quad (\text{C.22})$$

Differentiating $\rho(t) = e^{A(t)}/\mathcal{Z}(t)$ gives

$$\frac{d}{dt} \rho(t) = \frac{d}{dt} \left(e^{A(t)} \cdot \frac{1}{\mathcal{Z}(t)} \right) = F(t) - \rho(t) \text{Tr}[F(t)], \quad (\text{C.23})$$

where

$$F(t) = \frac{1}{\mathcal{Z}(t)} \frac{d}{dt} e^{A(t)} = \int_0^1 \rho(t)^s E \rho(t)^{1-s} ds. \quad (\text{C.24})$$

By Lemma S2, $\|F(t)\|_1 \leq \|E\|_\infty$. In addition,

$$\text{Tr}[F(t)] = \int_0^1 \text{Tr}[\rho(t)^s E \rho(t)^{1-s}] ds = \int_0^1 \text{Tr}[\rho(t) E] ds = \text{Tr}[\rho(t) E] \leq \|E\|_\infty. \quad (\text{C.25})$$

Therefore $\|\frac{d}{dt} \rho(t)\|_1 \leq 2\|E\|_\infty$ for all $t \in [0, 1]$, and integrating over t yields

$$\|\rho(1) - \rho(0)\|_1 \leq 2\|E\|_\infty, \quad (\text{C.26})$$

as claimed. \blacksquare

The main error bound is stated and proved below. The argument is most informative when indices repeat frequently (i.e., $N \gg \max(L, n)$), where the palindromic product can be compared sharply with an exponential via higher-order BCH control, yielding a tighter bound than a second-order Trotter decomposition [42].

Theorem 1 (Complete version) *Let $N = \Omega(n\lambda^2\beta^2)$ and $\delta > 0$. Then ρ_N in Equation (C.3) and $G_{\beta,H}$ in Equation (C.6) satisfy*

$$\Pr\left(\|\rho_N - G_{\beta,H}\|_1 > \mathcal{O}\left(K_0^{3/2} N^{3/2} \tau^3\right)\right) \leq \delta \quad (\text{C.27})$$

for $K_0 = (n+2) \log 2 + \log(N/\delta)$.

Proof Denote $S_k = \sum_{i=1}^k B_i$. By Lemma S10,

$$E := 2S_N - \log \left(\left(\prod_{k=N}^2 e^{B_k} \right) e^{2B_1} \left(\prod_{k=2}^N e^{B_k} \right) \right) = \frac{1}{3} (E_1 - 2E_2) - R_N \quad (\text{C.28})$$

for $E_1 = \sum_{k=2}^N [B_k, [B_k, S_{k-1}]]$, $E_2 = \sum_{k=2}^N [S_{k-1}, [B_k, S_{k-1}]]$ and some remainder term R_N . Lemma S11 reduces the trace-norm comparison to a spectral-norm bound on E :

$$\|\rho_N - G_{\beta, H}\|_1 = \left\| \frac{e^{\log(\prod_{k=N}^2 e^{B_k}) e^{2B_1} (\prod_{k=2}^N e^{B_k})}}{\text{Tr[same above]}} - \frac{e^{E + \log(\prod_{k=N}^2 e^{B_k}) e^{2B_1} (\prod_{k=2}^N e^{B_k})}}{\text{Tr[same above]}} \right\|_1 \leq 2\|E\|_\infty. \quad (\text{C.29})$$

It therefore suffices to upper bound $\|E_1\|_\infty$, $\|E_2\|_\infty$, and $\|R_N\|_\infty$ with high probability, and then combine these bounds.

We begin by controlling $\|S_k\|_\infty$. Let $\mathcal{F}_k = (B_i)_{i=1}^k$ be the natural filtration, define the drift $D_k = \mathbb{E}[B_k | \mathcal{F}_{k-1}]$, and let $M_k = B_k - D_k$. Then $S_k = \sum_{i=1}^k D_i + \sum_{i=1}^k M_i$. For the drift term, we have

$$\|D_k\|_\infty = \|\mathbb{E}[B_k | \mathcal{F}_{k-1}]\|_\infty = \left\| \left[\frac{\text{Tr}[e^{\tau\sigma_{j_k} \rho_{k-1}}]}{2 \cosh \tau} - \frac{\text{Tr}[e^{-\tau\sigma_{j_k} \rho_{k-1}}]}{2 \cosh \tau} \right] \cdot \frac{\tau\sigma_{j_k}}{2} \right\|_\infty \quad (\text{C.30})$$

$$\leq |\text{Tr}[e^{\tau\sigma_{j_k} \rho_{k-1}}] - \text{Tr}[e^{-\tau\sigma_{j_k} \rho_{k-1}}]| \cdot \frac{\tau}{4 \cosh \tau} \quad (\text{C.31})$$

$$= |(e^\tau - e^{-\tau}) \text{Tr}[\sigma_{j_k} \rho_{k-1}]| \cdot \frac{\tau}{2(e^\tau + e^{-\tau})} \quad (\text{C.32})$$

$$\leq \frac{1}{2} \tau \tanh \tau = \tau^2 + \mathcal{O}(\tau^4) < 0.1\tau, \quad (\text{C.33})$$

for $\tau \ll 1$. The sequence $(M_k)_k$ is a martingale difference sequence of Hermitian matrices with respect to $(\mathcal{F}_k)_k$, since $\mathbb{E}[M_k | \mathcal{F}_{k-1}] = 0$. In particular, $\|M_k\|_\infty \leq \|B_k\|_\infty + \|D_k\|_\infty \leq \tau + 0.1\tau = 1.1\tau$. Applying Lemma S4, for any k and $t_k > 0$,

$$\Pr\left(\left\|\sum_{i=1}^k M_i\right\|_\infty > t_k \text{ and } \left\|\sum_{i=1}^k \mathbb{E}[M_i^2 | \mathcal{F}_{i-1}]\right\|_\infty \leq \frac{k\tau^2}{4}\right) \leq 2^{n+1} \exp\left(-\frac{t_k^2/2}{k\tau^2/4 + 1.1\tau t_k/3}\right). \quad (\text{C.34})$$

We also have

$$\sum_{i=1}^k \mathbb{E}[M_i^2 | \mathcal{F}_{i-1}] = \sum_{i=1}^k \mathbb{E}[B_i^2 | \mathcal{F}_{i-1}] - D_i^2 = \sum_{i=1}^k \frac{\tau^2}{4} I - D_i^2 \quad (\text{C.35})$$

$$\implies \left\|\sum_{i=1}^k \mathbb{E}[M_i^2 | \mathcal{F}_{i-1}]\right\|_\infty \leq \sum_{i=1}^k \left\|\frac{\tau^2}{4} I - D_i^2\right\|_\infty \leq \sum_{i=1}^k \left\|\frac{\tau^2}{4} I\right\|_\infty = \frac{k}{4} \tau^2, \quad (\text{C.36})$$

so choosing $K = (n+1) \log 2 + \log \delta^{-1}$ and $t_k = \tau \sqrt{kK/2} + 2.2\tau K/3$ implies $(t_k/\tau)^2 / (k/2 + \frac{2.2}{3} t_k/\tau) \geq K$, and therefore

$$\Pr\left(\left\|\sum_{i=1}^k M_i\right\|_\infty > t_k\right) \leq 2^{n+1} \exp\left(-\frac{t_k^2}{k\tau^2/2 + 2.2\tau t_k/3}\right) = 2^{n+1} \exp\left(-\frac{(t_k/\tau)^2}{k/2 + 2.2/3 \cdot (t_k/\tau)}\right) \quad (\text{C.37})$$

$$\leq 2^{n+1} e^{-K} = \delta. \quad (\text{C.38})$$

Combining the drift and martingale parts yields

$$\|S_k\|_\infty \leq \left\|\sum_{i=1}^k M_i\right\|_\infty + \sum_{i=1}^k \|D_i\|_\infty \implies \Pr(\|S_k\|_\infty > t_k + k\tau^2) \leq \delta. \quad (\text{C.39})$$

We next bound $\|E_1\|_\infty$. Since $B_k \sim \{\tau\sigma_{j_k}/2, -\tau\sigma_{j_k}/2\}$,

$$\|E_1\|_\infty = \left\|\sum_{k=2}^N [B_k, [B_k, S_{k-1}]]\right\|_\infty \quad (\text{C.40})$$

$$\leq \sum_{k=2}^N \|[B_k, [B_k, S_{k-1}]]\|_\infty = \sum_{k=2}^N \|B_k^2 S_{k-1} + S_{k-1} B_k^2 - 2B_k S_{k-1} B_k\|_\infty \quad (\text{C.41})$$

$$= \frac{\tau^2}{2} \sum_{k=2}^N \|S_{k-1} - \sigma_{j_k} S_{k-1} \sigma_{j_k}\|_\infty \leq \tau^2 \sum_{k=2}^N \|S_{k-1}\|_\infty \quad (\text{C.42})$$

$$\implies \Pr\left(\|E_1\|_\infty > \tau^2 \sum_{k=2}^N (t_k + k\tau^2)\right) \leq \delta. \quad (\text{C.43})$$

The term E_2 is handled in a similar way. Assume $\|S_k\|_\infty \leq t_k + k\tau^2$ (we account for this event in the final probability bound). Define $Q_k = [S_k, [M_{k+1}, S_k]]$, so that

$$[S_{k-1}, [B_k, S_{k-1}]] = Q_{k-1} + [S_{k-1}, [D_k, S_{k-1}]] \quad (\text{C.44})$$

with $\|[S_{k-1}, [D_k, S_{k-1}]]\|_\infty \leq 4\|S_k\|_\infty^2 \|D_{k+1}\|_\infty = 4(t_k + k\tau^2)^2 \tau^2$. One can verify that $\mathbb{E}[Q_k | \mathcal{F}_k] = 0$ and

$$\|Q_k\|_\infty \leq 4\|S_k\|_\infty^2 \|M_{k+1}\|_\infty = 4.4(t_k + k\tau^2)^2 \tau, \quad (\text{C.45})$$

$$\|\mathbb{E}[Q_k^2 | \mathcal{F}_{k-1}]\|_\infty \leq 4\|S_k\|_\infty^4 \|M_{k+1}\|_\infty^2 \leq 20(t_k + k\tau^2)^4 \tau^2, \quad (\text{C.46})$$

$$\left\| \sum_{k=1}^N \mathbb{E}[Q_k^2 | \mathcal{F}_{k-1}] \right\|_\infty \leq 20N(t_N + N\tau^2)^4 \tau^2. \quad (\text{C.47})$$

Lemma S4 therefore implies that, for any k and $s_k > 0$,

$$\Pr\left(\left\| \sum_{i=1}^k Q_i \right\|_\infty > s_k\right) \leq 2^{n+1} \exp\left(-\frac{s_k^2/2}{20N(t_N + N\tau^2)^4 \tau^2 + 4.4(t_k + k\tau^2)^2 \tau s_k/3}\right). \quad (\text{C.48})$$

Taking $s_k = \sqrt{40KN}(t_N + N\tau^2)^2 \tau + 8.8(t_k + k\tau^2)^2 K\tau/3$ simplifies the bound to

$$\Pr\left(\left\| \sum_{i=1}^k Q_i \right\|_\infty > s_k\right) \leq 2^{n+1} e^{-K} \leq \delta. \quad (\text{C.49})$$

Consequently,

$$\|E_2\|_\infty = \left\| \sum_{k=2}^N [S_{k-1}, [B_k, S_{k-1}]] \right\|_\infty \leq \left\| \sum_{k=2}^N Q_{k-1} \right\|_\infty + \sum_{k=2}^N \|[S_{k-1}, [D_k, S_{k-1}]]\|_\infty \quad (\text{C.50})$$

$$\implies \Pr\left(\|E_2\|_\infty > s_N + 4 \sum_{k=2}^N (t_k + k\tau^2)^2 \tau^2\right) \leq \delta. \quad (\text{C.51})$$

We now combine the bounds. Since $N \gg n$, for all $k \leq N$ we have $t_k + k\tau^2 \leq t_N + N\tau^2 = \mathcal{O}(\tau\sqrt{NK}) + N\tau^2 = \mathcal{O}(\tau\sqrt{NK})$. Therefore, $\|E_1\|_\infty \leq \tau^2 \sum_{k=2}^N (t_k + k\tau^2) = \mathcal{O}(N\tau^3\sqrt{NK})$ and $\|E_2\|_\infty \leq s_N + 4 \sum_{k=2}^N (t_k + k\tau^2)^2 \tau^2 = \mathcal{O}(\tau^3 K^{3/2} N^{3/2})$, which implies $\|E_1 - 2E_2\|_\infty = \mathcal{O}(\tau^3 K^{3/2} N^{3/2})$.

It remains to bound the remainder term. By Lemma S10,

$$\|\mathcal{R}_N\|_\infty = \mathcal{O}\left(\sum_{r=5, r \text{ is odd}}^{\infty} \frac{1}{r!} \sum_{k=2}^N \|\text{ad}_{2S_{k-1}}^{r-1}(B_k)\|_\infty\right). \quad (\text{C.52})$$

For an odd order $r \geq 5$, applying Lemma S4 yields

$$\frac{1}{r!} \sum_{k=2}^N \|\text{ad}_{2S_{k-1}}^{r-1}(B_k)\|_\infty = \frac{2^r}{r!} \mathcal{O}\left((\sqrt{NK}\tau)^r\right) = o(\tau^3 K^{3/2} N^{3/2}). \quad (\text{C.53})$$

Alternatively, the triangle inequality gives

$$\frac{1}{r!} \sum_{k=2}^N \|\text{ad}_{2S_{k-1}}^{r-1}(B_k)\|_\infty = \frac{2^{2r}}{r!} \mathcal{O}\left(N\tau(\sqrt{NK}\tau)^{r-1}\right). \quad (\text{C.54})$$

For $r^* = \left\lceil \frac{\log(K\tau^2\sqrt{NK})}{\log(\tau\sqrt{NK})} \right\rceil$, this implies $\|\mathcal{R}_N\|_\infty = \mathcal{O}(\tau^3 K^{3/2} N^{3/2})$. We therefore apply Lemma S4 for $r < r^*$ and use the triangle inequality for $r \geq r^*$; the remaining tail ($r > r^*$) decays exponentially and can be neglected at the stated precision.

Substituting these bounds into $\|\rho_N - G_{\beta,H}\|_1 \leq 2\|E\|_\infty$ yields

$$\Pr\left(\|\rho_N - G_{\beta,H}\|_1 \leq \mathcal{O}\left(K^{3/2}N^{3/2}\tau^3\right)\right) \geq 1 - \delta. \quad (\text{C.55})$$

It remains to account for the overall failure probability. The proof applies Lemma S4 $(r^* - 1)/2 + N$ times. Setting $\delta' = \delta/((r^* - 1)/2 + N)$ and taking a union bound ensures that the total failure probability is at most δ . Under this rescaling, $K = (n + 1)\log 2 + \log(((r^* - 1)/2 + N)/\delta)$. Given $N \gg n$ and $\tau\sqrt{NK} \ll 1$, we may assume $N \gg K$ and obtain

$$r^* \leq 2 + \frac{\log(K\tau)}{\log(\tau\sqrt{NK})} \ll N, \quad (\text{C.56})$$

which implies $K \leq (n + 2)\log 2 + \log(N/\delta) \ll N$. Taking $K_0 = (n + 2)\log 2 + \log(N/\delta)$ therefore yields the stated bound. ■

2. Sample distribution

Recall that Algorithm 1 generates a path $\mathcal{P} = ((j_1, m_1), \dots, (j_N, m_N)) \in [L] \times \{1, -1\}$. In Section C 1, we assumed \mathcal{P} is fixed so that the evolution sequence can be analyzed without randomness. This section uses a random walk to incorporate the randomness of j_k and m_k .

Consider how the sampled Hamiltonian evolves as the path develops. Stopping the algorithm at step $k \in [N]$ yields the intermediate Hamiltonian $H^{(k)} = \sum_{t=1}^k m_t \sigma_{j_t}$. The sampling process can thus be described as a sequence $(H^{(k)})_k$, with $H^{(N)}$ being the final output. Equivalently, this sequence is a random walk on a lattice:

$$\mathbf{x}^{(k)} = \sum_{t=1}^k m_t e_{j_t} \in \{-N, \dots, N\}^{\times L}, \quad \mathbf{x}^{(0)} = 0, \quad (\text{C.57})$$

where e_{j_t} is the standard vector in the lattice corresponding to σ_{j_t} , and every forward step satisfies

$$\Pr\left(\mathbf{x}^{(k)} - \mathbf{x}^{(k-1)} = \pm e_j\right) = \Pr(m_k = \pm 1) \cdot h_j/\lambda. \quad (\text{C.58})$$

The sign of m_k is determined by the quantum measurement in Theorem S7, which is difficult to analyze directly. We therefore introduce a reference probability measure Q with $\Pr_Q(m_k = \pm 1) = 1/2$, giving

$$\Pr_Q\left(\mathbf{x}^{(k)} - \mathbf{x}^{(k-1)} = \pm e_j\right) = h_j/2\lambda \quad (\text{C.59})$$

corresponding to $N \rightarrow \infty$. The relation between the reference probability measure and the true probability measure is stated by the likelihood ratio $L_N(\mathcal{P}) = \Pr(\mathcal{P})/\Pr_Q(\mathcal{P})$ in the following statement.

Lemma S13 *If $N = \Omega(n\lambda^2\beta^2)$, then for $H = H^{(N)}$,*

$$\log L_N(\mathcal{P}) = \log\left(\frac{1}{2^n} \text{Tr}[e^{-\beta H}]\right) + \mathcal{O}\left(\frac{\lambda^2\beta^2}{N}\right). \quad (\text{C.60})$$

Proof For convenience, denote $\rho_{\mathbf{x}}$ as the thermal state of Hamiltonian with respect to \mathbf{x} and $M_j(\mathbf{x}) = \text{Tr}[\sigma_j \rho_{\mathbf{x}}]$. By Theorem S7, the outcome distribution at step t given the Pauli operator σ_{j_t} can be written as

$$\Pr(m_t = \pm 1 \mid j_t) = \frac{1}{2} \left(1 \mp \tanh \tau \text{Tr}[\sigma_{j_t} M_{j_t}(\mathbf{x}^{(t-1)})]\right) \quad (\text{C.61})$$

Since $\Pr_Q(m_t = \pm 1 \mid j_t) = 1/2$ and the probabilities for sampling j_t for both measures are the same, the likelihood ratio takes the product form

$$L_N(\mathcal{P}) = 2^N \prod_{t=1}^N \Pr(m_t = \pm 1 \mid j_t) = \prod_{t=1}^N \left(1 - m_t \tanh(\tau) M_{j_t}(\mathbf{x}^{(t-1)})\right). \quad (\text{C.62})$$

Using $\log(1+y) = y + \mathcal{O}(y^2)$ and $\tanh \tau = \tau + \mathcal{O}(\tau^3)$ gives

$$\log L_N(j, m) = -\tau \sum_{t=1}^N m_t M_{j_t}(\mathbf{x}^{(t-1)}) + \mathcal{O}(N\tau^2). \quad (\text{C.63})$$

Denote the partition function of $H^{(t)}$ at the t -th step as

$$\mathcal{Z}(\mathbf{x}^{(t)}) = \text{Tr} \left[\exp(-\beta H^{(t)}) \right] = \text{Tr} \left[\exp \left(-\tau \sum_{j=1}^L \mathbf{x}_j^{(t)} \sigma_j \right) \right]. \quad (\text{C.64})$$

Observe that differentiating $\log \mathcal{Z}(\mathbf{x})$ with respect to \mathbf{x}_j gives

$$\partial_{\mathbf{x}_j} \log \mathcal{Z}(\mathbf{x}) = \frac{1}{\mathcal{Z}(\mathbf{x})} \text{Tr} \left[(-\tau \sigma_j) \exp \left(-\tau \sum_{j=1}^L \mathbf{x}_j \sigma_j \right) \right] = -\tau M_j(\mathbf{x}). \quad (\text{C.65})$$

Therefore, since $\mathbf{x}^{(t)} - \mathbf{x}^{(t-1)} = m_t e_{j_t}$,

$$-\tau m_t M_{j_t}(\mathbf{x}^{(t-1)}) = m_t \partial_{\mathbf{x}^{(t-1)}} \log \mathcal{Z}(\mathbf{x}^{(t-1)}) = \nabla_{\mathbf{x}} \log \mathcal{Z}(\mathbf{x}^{(t-1)}) \cdot (\mathbf{x}^{(t)} - \mathbf{x}^{(t-1)}). \quad (\text{C.66})$$

Because $\mathcal{Z}(\mathbf{x})$ depends on \mathbf{x} through $\tau \mathbf{x}$ and $\tau \ll 1$, a Taylor expansion of $\log \mathcal{Z}$ along one lattice step gives

$$\log \mathcal{Z}(\mathbf{x}^{(t)}) - \log \mathcal{Z}(\mathbf{x}^{(t-1)}) = \nabla_{\mathbf{x}} \log \mathcal{Z}(\mathbf{x}^{(t-1)}) \cdot (\mathbf{x}^{(t)} - \mathbf{x}^{(t-1)}) + \mathcal{O}(\tau^2). \quad (\text{C.67})$$

Summing over $t = 1, \dots, N$ and substituting into Equation (C.63) yields

$$\log L_N(j, m) = \log \mathcal{Z}(\mathbf{x}^{(N)}) - \log \mathcal{Z}(0) + \mathcal{O}(N\tau^2). \quad (\text{C.68})$$

Finally, $\mathcal{Z}(0) = \text{Tr}[I] = 2^n$ and $\mathcal{Z}(\mathbf{x}^{(N)}) = \text{Tr} \left[\exp(-\tau \sum_j \mathbf{x}_j \sigma_j) \right] = \text{Tr} \left[e^{-\beta H^{(N)}} \right]$, so the statement follows from $N\tau^2 = \lambda^2 \beta^2 / N$. \blacksquare

We now state the theoretical result for the sample distribution.

Theorem 2 (Complete version) *Suppose $n \gg 1$ and $N = \Omega(n\lambda^2\beta^2)$. Let $H = \sum_{j=1}^L c_j \sigma_j$ and $p_j = c_j / \lambda$. When $\sum_j c_j^2 \leq N\lambda^2$, the datum $(G_{\beta, H}, H)$ can be sampled by Algorithm 1 with probability proportional to $\frac{1}{2^n} \text{Tr} [e^{-\beta H}] \cdot D(\mathbf{x})$, where D is given as*

$$D(\mathbf{x}) = \frac{a_N(\mathbf{x})}{(2\pi N)^{L/2} \sqrt{\prod_{j=1}^L p_j}} \exp \left(-\frac{1}{2N} \sum_j p_j \mathbf{x}_j^2 \right) + o(N^{-L/2}). \quad (\text{C.69})$$

Proof Fix $H = \sum_{j=1}^L c_j \sigma_j$ on the output grid, and let $\mathbf{x} \in \mathbb{Z}^L$ be the corresponding endpoint vector $\mathbf{x}_j = c_j N / \lambda$. Denote $\mathcal{P}_{\mathbf{x}}$ the set of paths whose endpoint equals \mathbf{x} . Then the event that Algorithm 1 returns H is exactly the endpoint event $\mathbf{x}^{(N)} = \mathbf{x}$.

By definition of the likelihood ratio and Lemma S13,

$$\Pr(\mathcal{P}) = \Pr_Q(\mathcal{P}) \cdot \exp \left(\log \left(\frac{1}{2^n} \text{Tr} [e^{-\beta H}] \right) + \mathcal{O} \left(\frac{\lambda^2 \beta^2}{N} \right) \right). \quad (\text{C.70})$$

When $\|\mathbf{x}\| = \mathcal{O}(\sqrt{N})$. Therefore, absorbing the \mathbf{x} -independent normalization into the proportionality constant, summing over all \mathcal{P} with same endpoint, we obtain

$$\begin{aligned} \Pr(\mathbf{x}^{(N)} = \mathbf{x}) &= \exp \left(\log \left(\frac{1}{2^n} \text{Tr} [e^{-\beta H}] \right) + \mathcal{O} \left(\frac{\lambda^2 \beta^2}{N} \right) \right) \cdot \sum_{\mathcal{P} \in \mathcal{P}_{\mathbf{x}}} \Pr_Q(\mathcal{P}) \\ &\propto \frac{1}{2^n} \text{Tr} [e^{-\beta H}] \cdot \Pr_Q(\mathbf{x}^{(N)} = \mathbf{x}). \end{aligned} \quad (\text{C.71})$$

Denote $D(\mathbf{x}) = \Pr_Q(\mathbf{x}^{(N)} = \mathbf{x})$. Substituting Lemma S5 yields the Gaussian approximation claimed in the theorem. \blacksquare

Appendix D: Application details

1. Level statistics of quantum density operators

This section outlines the framework for analyzing the spectral properties of the generated quantum thermal states, which we use as a benchmark for whether the sampler captures nontrivial chaotic correlations. Level statistics, commonly applied to Hamiltonian energy spectra to diagnose quantum chaos and ergodicity [46, 50], extend naturally to density operators ρ via the modular Hamiltonian.

For a strictly positive density operator ρ , its spectral properties are closely related to those of the fictitious Hamiltonian governing the thermal distribution. We define the modular Hamiltonian H by $\rho = \frac{e^{-H}}{\text{Tr}(e^{-H})}$. The eigenvalues of ρ , denoted by $\{p_i\}$, are directly related to the spectrum of H , denoted by $\{\xi_i\}$, via the transformation $\xi_i = -\ln(p_i) - \ln Z$. The level statistics of ρ are thus analyzed through the unfolding of the "entanglement energies" or modular levels $\{\xi_i\}$.

To avoid the ambiguities associated with spectral unfolding in finite-size systems, we utilize the adjacent gap ratio statistics introduced by O'Ganesyan and Huse [46]. Let the sorted spectrum of the modular Hamiltonian be ordered such that $\xi_1 \leq \xi_2 \leq \dots \leq \xi_D$, where D is the dimension of the Hilbert space. We define the nearest-neighbor level spacing as:

$$\delta_n = \xi_{n+1} - \xi_n \geq 0. \quad (\text{D.1})$$

The dimensionless level spacing ratio r_n is defined as:

$$r_n = \frac{\min(\delta_n, \delta_{n+1})}{\max(\delta_n, \delta_{n+1})} = \min\left(\tilde{r}_n, \frac{1}{\tilde{r}_n}\right) \in [0, 1] \quad (\text{D.2})$$

where $\tilde{r}_n = \delta_{n+1}/\delta_n$. The distribution of r_n , denoted as $P(r)$, and its mean value $\langle r \rangle$, serve as robust indicators of the nature of the correlations in the quantum state. The following summarizes the known results of the average spacing ratios with respect to the specific RMT ensembles [67]:

- *Integrable (Poissonian) limit:* Systems with uncorrelated levels, typical of integrable models or localized phases, exhibit level spacings following a Poisson distribution with $P(r) = \frac{2}{(1+r)^2}$ and $\langle r \rangle_{\text{Poisson}} \approx 0.386$.
- *Chaotic (Wigner–Dyson) limit:* Ergodic quantum systems exhibit level repulsion characteristic of Random Matrix Theory (RMT), with statistics depending on the symmetry class: $\langle r \rangle_{\text{GOE}} \approx 0.536$ for systems with time-reversal symmetry, and $\langle r \rangle_{\text{GUE}} \approx 0.603$ for systems without.

In our algorithm, $\langle r \rangle$ values approaching the GUE/GOE limits in the sampled thermal states indicate that the generated state captures the complexity and correlations of a thermalizing many-body system. Conversely, $\langle r \rangle \approx 0.39$ would suggest a failure to capture thermal correlations or an underlying integrability in the generator set.

2. State classification by Hamiltonian properties

Let us specify the background first. Let Σ and h be as defined in Section C that describe a set of Hamiltonians \mathfrak{H} . For a label function $f : \mathfrak{H} \rightarrow \{0, 1\}$ that divide this set to group 0 and group 1, given access to an unknown thermal state $G_{\beta, H}$ (with known temperature β), the goal of state classification is to predict whether $f(H)$ is 0 or 1. Denote the labelled set $D_y = \{\rho : (\rho, H) \in S(\beta, \Sigma, h), f(H) = y\}$ for $y = 0, 1$, and without loss of generality, suppose $|D_0| = |D_1|$. Then, equivalently, we are looking for an n -to-1 channel \mathcal{E} that maximizes the average success probability of prediction

$$P(\mathcal{E}) = \frac{1}{2} \sum_{y=0}^1 \Pr(\text{predict } y \mid \rho \in D_y) = \frac{1}{2} \sum_{y=0}^1 \int_{D_y} \text{Tr}[\mathcal{E}(\rho) \cdot |0\rangle\langle 0|] \, d\rho = \frac{1}{2} \sum_{y=0}^1 \text{Tr}[\mathcal{E}(\rho_y) \cdot |y\rangle\langle y|] \quad (\text{D.3})$$

for $\rho_y = \int_{D_y} \rho \, d\rho$ is the average mixture of the state set D_y , and $\rho_y = \frac{1}{|D_y|} \sum_{\rho \in D_y} \rho$ when D_y is finite. Theoretically, this average success probability of prediction is upper bounded by the Helstrom limit [57],

$$P(\mathcal{E}) \leq \frac{1}{2}(1 + \|\rho_0 - \rho_1\|_1). \quad (\text{D.4})$$

In later experiment, the Helstrom limit is used to evaluate the convergence performance.

The rest of this section outlines an example training algorithm on how to use our sampler as data source to find a protocol to tackle this task. In the standard expectation-value-based formulation, each loss evaluation typically requires many circuit repetitions on the same input state; here we instead use single-shot outcomes on freshly sampled batches from the stochastic data source. We model the n -to-1 channel \mathcal{E} by an $(n + 1)$ -qubit parameterized quantum circuit [56] $U(\theta)$ with one ancilla qubit. The circuit takes an n -qubit state ρ as input and traces out the main system; we denote the resulting parameterized channel as \mathcal{E}_θ . Then for a finite set of input state ρ_1, \dots, ρ_d that approximates thermal states $G_{\beta, H_1}, \dots, G_{\beta, H_d}$ generated by our sampler, respectively, and their 0/1 label vector $\hat{y} = (f(H_1), \dots, f(H_d)) \in \{0, 1\}^d$, the average prediction loss is defined as the stochastic function

$$\mathcal{L}(\theta) = \left(1 - \frac{1}{d} y(\theta) \cdot \hat{y}\right)/2, \quad \text{where } \Pr(y_i(\theta) = \hat{y}_i) = \text{Tr}[\mathcal{E}_\theta(G_{\beta, H_i}) \cdot |f(H_i)\rangle\langle f(H_i)|] \quad (\text{D.5})$$

such that the expectation is the average failure probability of prediction,

$$\mathbb{E}[\mathcal{L}(\theta)] = 1 - \frac{1}{d} \sum_{i=1}^d \text{Tr}[\mathcal{E}_\theta(G_{\beta, H_i}) \cdot |f(H_i)\rangle\langle f(H_i)|]. \quad (\text{D.6})$$

Then our objective is to find the optimal parameters $\theta^* = \arg \min_\theta \mathbb{E}[\mathcal{L}(\theta)]$. Since $\mathcal{L}(\theta)$ is stochastic, we estimate the gradient using a stochastic variant of the parameter-shift rule [58, 59]. Unlike the standard formulation based on expectation-value estimation, each loss evaluation here is obtained from single-shot measurements on a freshly sampled batch. For each parameter θ_j associated with a Pauli-rotation gate $U(\theta_j) = \exp(-i\theta_j P/2)$, the gradient component can be estimated by

$$\nabla_j \mathcal{L}(\theta) = \frac{\mathcal{L}(\theta + \frac{\pi}{2} e_j) - \mathcal{L}(\theta - \frac{\pi}{2} e_j)}{2}, \quad (\text{D.7})$$

where e_j is the unit vector in the j th coordinate. This estimator is unbiased in the presence of a stochastic data source, i.e., $\mathbb{E}[\nabla \mathcal{L}(\theta)] = \nabla \mathbb{E}[\mathcal{L}(\theta)]$. The complete training procedure is summarized in Algorithm 2. Here ϵ controls the sampling precision of our sampler, and w is a weight function that controls the importance of each Hamiltonian.

Algorithm 2: Training a parameterized quantum circuit for state classification

Input : A label function f , inverse temperature β , a set Σ of n -qubit Pauli operators with boundary vector h , precision ϵ , training steps T , batch size d , learning rate γ , weight function $w(H) \in \mathbb{R}_+$

Output: A channel \mathcal{E} that approximately maximizes $P(\mathcal{E})$ in Equation (D.3)

```

1  $N \leftarrow \lambda^2 \beta^2 \epsilon^{-2/3}$ ;
2 SAMPLE  $\leftarrow$  Algorithm 1 with inputs  $\beta, \Sigma, h, N$ ;
3 Choose a circuit ansatz  $U(\theta)$  with random parameters  $\theta$ , and define  $\mathcal{E}_\theta \leftarrow \text{Tr}_{\text{sys}}[U(\theta) (|0\rangle\langle 0|_{\text{anc}} \otimes (\cdot)_{\text{sys}}) U(\theta)^\dagger]$ ;
4 for  $t = 1, \dots, T$  do
5    $g \leftarrow 0^{|\theta|}$ ;
6   for  $j = 1, \dots, |\theta|$  do
7     for  $s \in \{+1, -1\}$  do
8       for  $i = 1, \dots, d$  do
9          $(\rho_i, H_i) \leftarrow \text{SAMPLE}()$ ;
10         $y_i \leftarrow \text{measure } \mathcal{E}_{\theta + s \cdot \frac{\pi}{2} e_j}(\rho_i), \hat{y}_i \leftarrow f(H_i)$ ;
11         $\mathcal{L}_s \leftarrow (1 - \sum_i w(H_i) y_i \hat{y}_i / \sum_i w(H_i)) / 2$ ;
12       $g_j \leftarrow (\mathcal{L}_{+1} - \mathcal{L}_{-1}) / 2$ ;
13    $\theta \leftarrow \theta - \gamma \cdot g$  (or use Adam optimizer);
14 return  $\mathcal{E} = \mathcal{E}_\theta$ 

```

The convergence of Algorithm 2 depends on the variance of the parameter-shift gradient estimate. Since each iteration requires $2|\theta|$ stochastic loss evaluations, both the evaluation budget and the batch size d affect the gradient noise in the presence of data and measurement sampling. If d is not large enough, the variance may be too high for the classifier to converge. The weight function w adjusts the loss in Equation (D.5) to emphasize Hamiltonians whose importance is not too small, thereby improving the effective signal-to-noise ratio.

Appendix E: Experimental setting

Figure 2-3a

All experiments for Figure 2 and Figure 3a are performed on a 3×3 two-dimensional grid of $n = 9$ qubits, with sites labeled $1, \dots, 9$ in row-major order. The nearest-neighbor pairs $\langle i, j \rangle$ consist of 12 edges connecting horizontally and vertically adjacent sites. For the Heisenberg model, the sampled Hamiltonians take the form

$$H_{\text{Heis}} = \sum_{\langle i, j \rangle} \left(c_{ij}^{(X)} X_i X_j + c_{ij}^{(Y)} Y_i Y_j + c_{ij}^{(Z)} Z_i Z_j \right), \quad (\text{E.1})$$

where the coefficients $c_{ij}^{(\alpha)}$ are generated by the sampling algorithm and satisfy $|c_{ij}^{(\alpha)}| \leq h$ for a uniform bound $h > 0$. For the transverse-field Ising model, the sampled Hamiltonians take the form

$$H_{\text{Ising}} = \sum_{\langle i, j \rangle} c_{ij} Z_i Z_j + \sum_{i=1}^n g_i X_i, \quad (\text{E.2})$$

where the coefficients c_{ij} and g_i are similarly bounded. In both cases, $\lambda = \sum_j h_j$ denotes the sum of all coefficient bounds. Throughout, we set the step-number constant $C = \lambda^2 / \epsilon_0^{2/3}$ with target precision $\epsilon_0 = 10^{-6}$.

For Figure 2, all three panels use the Heisenberg model with the maximally mixed state I/d as the initial state. In panel (a), we scan the inverse temperature from $\beta = 1$ to $\beta = 10$ and test three scaling exponents $k \in \{1.5, 2.0, 2.5\}$, which define the step number as $N = C\beta^k$. For each parameter pair (β, N) , we perform 100 independent sampling runs and record the maximal trace-distance error ϵ among the samples. Panels (b) and (c) both fix $\beta = 2$. In panel (b), we set $N = C\beta^2$ and generate 10 000 independent samples to obtain the empirical coefficient distribution; the theoretical curve is computed from the normal distribution predicted by Theorem 2, reweighted by the thermal partition function and estimated via Monte Carlo with 10 000 samples. In panel (c), we scan the scaling exponent k from 1 to 3 and perform 100 independent runs for each $N = C\beta^k$. The inverse precision is defined as $1/\epsilon$, where ϵ is the maximal trace-distance error among the samples. The effective sample range is quantified by the operator norm $\|H\|_\infty$ of each sampled Hamiltonian; we report the sample mean and standard error over the thermal ensemble.

For Figure 3(a), we use the transverse-field Ising model to generate the output states. The initial state is a thermal state of a Heisenberg Hamiltonian, whose modular spectrum exhibits near-Poisson statistics in this finite-size setting. We fix $\beta = 2$ and $N = C\beta^2$, and perform 20 independent sampling runs. For each output state ρ , we define the modular Hamiltonian $K = -\log \rho$ and compute the adjacent gap-ratio statistic r from the spectrum of K . To handle near-degeneracies, eigenvalues within a relative tolerance of 10^{-6} are merged into a single representative level before evaluating the spacing ratios. The resulting r values are aggregated over all samples to form the final histogram.

Figure 3b

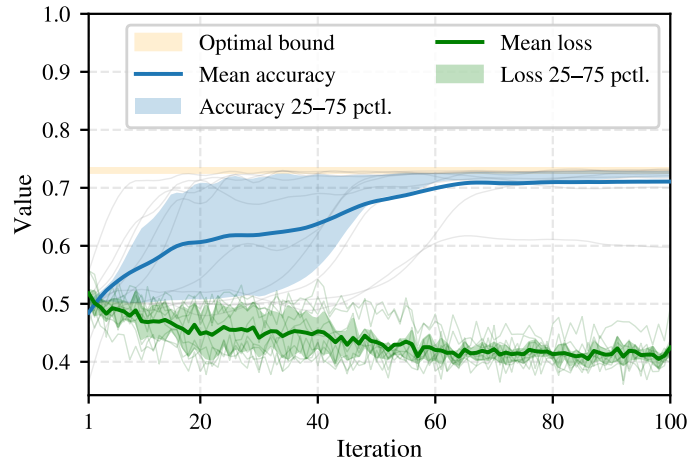
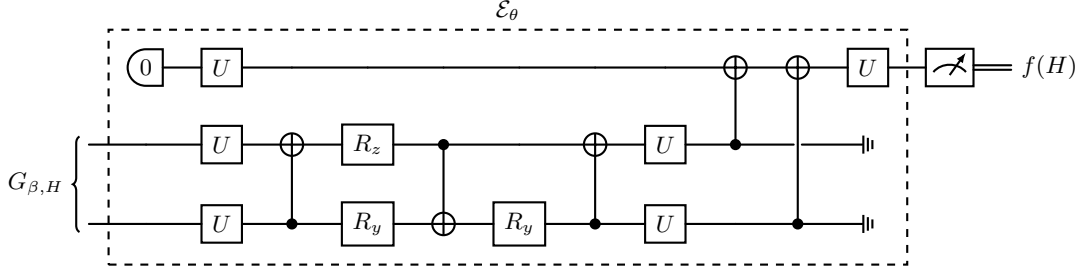


Fig S2. Training details for the state classification task, showing both accuracy and loss as functions of the training iteration.

The complete figure of Figure 3b, including loss values, is shown in Figure S2. In this experiment, we follow the procedure described in Section D 2 to classify two-qubit Hamiltonians by the sign of their $X \otimes X$ coefficient, using their thermal states at inverse temperature $\beta = 2$. The Hamiltonians take the form $H = h_1 X \otimes X + h_2 I \otimes Z + h_3 Z \otimes I$ with $|h_1|, |h_2|, |h_3| \leq 1$. We further restrict to Hamiltonians whose $X \otimes X$ coefficient satisfies $|h_1| \geq 0.03$. We run Algorithm 2 over 10 independent trials with the following setting:

- $f : H \mapsto h_1/|h_1|$,
- $\Sigma = \{X \otimes X, I \otimes Z, Z \otimes I\}$ with $h = (1, 1, 1)$,
- number of training step $T = 100$, number of training size $d = 1000$,
- parameter-shift value $\pi/2$, learning rate $\gamma = 0.1$,
- the weight function $w(H) = 0.05 + 0.95 \text{Sigmoid}((|h_1| - 0.01\lambda)/0.0025\lambda)$.

We choose the implementation of the variational quantum classifier to consist of a universal 2-qubit layer (built from parameterized single-qubit universal gates U and Pauli-rotation gates R_z, R_y) on the input state, together with two additional single-qubit universal gates on the ancilla before and after coupling it to the system, shown as follows.



For each independent trial, we also prepare a separate test set of size 3000 to evaluate the model at each training iteration. For each test set, we compute the Helstrom limit in Equation (D.4), which yields an upper bound of approximately 0.72–0.74. To assess generalization, the test set consists of exact thermal states with Hamiltonian coefficients h_1, h_2, h_3 sampled from a uniform distribution, in contrast to the training set whose approximate thermal states are sampled from the thermal-weighted normal distribution (Theorem 2). The performance metric is the average success probability of prediction defined in Equation (D.3).